

ACTAR

**An Active Target detector
for the study of extremely exotic nuclei**

June 19, 2009

Abstract

ACTAR is a new active target/time-projection chamber, designed for reaction and decay studies with nuclei far from stability. This class of instruments, initially developed for high-energy physics, has found profitable applications in medium- and low-energy nuclear physics as shown by a successful series of experiments. ACTAR builds on this experience to go beyond, incorporating developments in gas detector technology and a newly-designed electronic system of unprecedented scale in our research domain.

The physics cases for the new-generation active target are related to the ongoing developments of facilities for radioactive ion beams. Thanks to its flexibility, this instrument will be capable of taking advantage of the most exotic beams produced at in-flight fragmentation facilities, as well as the high-quality ISOL beams which will become available for example at SPIRAL2.

The interest in the active target project has been lively: a dedicated research activity within EURONS has brought together a large community, where the common aspects of various instruments were studied. An outcome of those studies has been the start of a project, now financed by the French ANR, for the realization of a general electronic system for active targets and time-projection chambers (acronym GET) for nuclear structure studies.

ACTAR, initially presented as a Letter of Intent to the SPIRAL2 project, will crucially benefit from the GET ANR, to which it is strongly linked. This and the recent addition of ACTAR to the SPIRAL2 Preparatory Phase (an FP7 project) provide the framework to consolidate the collaboration and start a programme that will lead to the construction of the new detector in a time frame of four years. This document illustrates the physics goals and technical aspects of ACTAR, and presents the plan of the project.

The ACTAR Collaboration

GANIL	A. Chbihi, F. de Oliveira, B. Dominguez Fernandez, J. Pancin, R. Raabe, T. Roger, P. Roussel-Chomaz, F. Saillant, H. Savajols, G. Wittwer
CEA/DSM/IRFU Saclay	S. Anvar, P. Baron, F. Druillole, A. Gillibert, L. Nalpas, L. Pollacco
CENBG	B. Blank, J. Giovinazzo, J. L. Pedroza, J. Pibernat
IPN Orsay	E. Khan, C. Petrache
LPC Caen	J. Gibelin, M. Marques, N. Orr
GSI	P. Egelhof
Andrzej Sołtan Institute	N. Keeley
Heavy Ion Laboratory - Warsaw University	K. Rusek
Henryk Niewodniczański Institute	R. Wolski
University of Santiago de Compostela	H. Alvarez-Pol, M. Caamaño, D. Cortina-Gil
University of Huelva	I. Martel
STFC Daresbury Laboratory	R. Lemmon
University of Surrey	W. Catford
University of Birmingham	M. Freer
University of Edinburgh	A. Murphy
University of Liverpool	M. Chartier
University of York	A. Laird
K.U. Leuven	M. Huyse, P. Van Duppen
ISOLDE, CERN	Y. Blumenfeld, J. Van de Walle
NSCL, MSU	W. Mittig

Contents

1	Introduction	7
1.1	Overview	7
1.2	Context of the ACTAR collaboration	8
2	Detector concept	10
2.1	Detection principle	10
2.2	Present active target detectors	12
2.3	ACTAR description and performances	14
3	Physics motivation	20
3.1	Opportunities with Radioactive Ion Beams	20
3.2	Elastic scattering	20
3.3	Spectroscopic studies with inelastic scattering and transfer reactions	21
3.4	Resonant reactions	22
3.5	Inelastic scattering and isoscalar giant resonances	23
3.6	Exotic decay modes at the driplines	24
4	Detailed physics cases	26
4.1	Transfer reactions on ^{78}Ni	26
4.2	Resonant reactions: $^{26}\text{Ne}+p$	31
4.3	Inelastic scattering and GRs: $^{56}\text{Ni}(\alpha, \alpha')$	33
4.4	Two-proton decay measurements	39
5	Design of the detector	41
5.1	Vacuum and gas system	42
5.2	Mechanics of the chamber	42
5.3	Field structure	43
5.4	Amplification technology	43
5.5	Anode	46
5.6	Ancillary detectors	48
5.7	Detection gases	49
5.8	Electronics and data acquisition: the GET project	51
6	Planning	54
6.1	Organisation - WBS	54
6.1.1	WP1 - Coordination	54
6.1.2	WP2 - Physics support	54
6.1.3	WP3 - Tests	56
6.1.4	WP4 - Detector design and assembly	57
6.1.5	WP5 - Documentation	58

6.2	Timeline	59
6.3	Resources	62
A	Energy loss of ions	65
	References	70

1 Introduction

1.1 Overview

About twenty years ago, experiments in nuclear physics started employing accelerated beams of unstable nuclei, having a large excess of protons or neutrons. In the years that followed and up to the present day, truly exotic properties were discovered in these nuclei. In some light systems, excess nucleons lead to large spatial extensions of the wave function, developing into halos [1]; configurations of clusters of nucleons give way to excitation patterns typical of molecular structures [2]. In heavier systems, the extreme neutron/proton ratio modifies profoundly the effective nucleon-nucleon interaction, leading to a break-down of shell closures and to different “magic numbers” [3]. Rare decay modes have been identified in dripline nuclei [4]. Such discoveries challenge our understanding of the nuclear structure, and have important consequences in related fields, such as nuclear astrophysics. New, more detailed experimental information, that can cast light on these questions, will be accessed by the concurrent developments in the production of radioactive ion beams and new detection systems. Here we present one of such systems.

Intensities of radioactive ion beams (RIBs) at the present facilities are much lower than in the case of stable beams, ranging from few particles/day to some 10^7 particles per second (pps); their optical qualities (beam size and emittance) are also often much poorer than for stable beams. To overcome these difficulties, new detection systems need to be developed, having high geometrical efficiency and fine spatial resolution. In order to further increase the reaction yields, thick targets are also required. This becomes a severe limiting factor as it leads to high energy losses and corresponding resolution degradation. In addition, since usually reactions are performed in inverse kinematics (a heavy projectile impinging on light target nuclei), the light recoil have a very low energy and are difficult to detect. These issues become even more important when using post-accelerated heavy secondary beams such as those that will become available at SPIRAL2, HIE-ISOLDE and ISAC2.

The idea of an active target, based on a gaseous ionization detector where the nuclei of the gas atoms are also the target nuclei, overcomes most of these difficulties. Gaseous detectors potentially have a very good geometric efficiency, a low detection threshold and excellent tracking capabilities (thus allowing the measurement of angular distributions); also, they have possibilities in particle identification. A large target thickness is possible without losing in resolution. In principle, the thickness can be increased to the point where the incident ion beam is completely stopped in the target, optimizing in this way the use of the exotic beam. The method offers also specific advantages: in case of short-leaving or unbound reaction products, the decay and its products can be detected in the gas volume itself; exploiting the energy loss of the incident beam in the gas, excitation functions can be obtained for selected reactions with

a single tuning of the accelerator, thus optimizing the beam time. Several results have already been obtained in measurements covering different physics cases, as reported in section 2.2.

The experience gained with the present active targets has led to the identification of a number of critical improvements, which we intend to implement in a new generation of such detectors. A significant amount of development has already taken place within the framework of various collaborations (section 1.2). We plan to continue this work, finalising the various aspects (mechanics, electronics, software), and build the new active target detector, ACTAR, in a time frame of about 4 years.

1.2 Context of the ACTAR collaboration

In the period 2005-2008, a broad research program on active target detectors has been carried out within the EURONS FP6 Joint Research Activity “ACTAR” [5]. As result, a number of documents were generated, which present in detail: the general physics motivations and specific physics cases; studies and tests around the possible solutions for the mechanics and detection technology; software developments for simulations and data analysis; characteristics and performances required for the electronics of the new generation of active targets.

The electronics in particular has been identified as a key element in the realization of future detectors of this kind. Because of a wide interest, an initiative for a specific development has been taken, in a form of a project aiming at building and testing a prototype of such an electronic system in a time frame of four years. The project name is GET (General Electronics for time-projection chambers, TPCs) [6]. A proposal to the French National Research Agency (ANR) was submitted in the fall of 2008 by IRFU Saclay, GANIL and CENBG, with MSU/NSCL participating as a foreign partner. The project has been accepted and almost fully financed. In the same context, a Memorandum of Understanding is in preparation between these laboratories (and the addition of RIKEN) to ensure a supporting structure to the future R&D activities.

GET is a flexible, generic system covering the electronics from the front-end cards (FEE) to the data acquisition and control (DAQ), which will instrument various active target and TPC detectors with different specific nuclear physics requirements and characteristics: The MSU active target (AT-TPC [7]), the SAMURAI TPC at RIKEN [8], the future version of the IKAR target at GSI, the R3B active target planned for FAIR [9]; and the ACTAR TPC for reaction and decay studies.

The latter was presented as a Letter of Intent to the SPIRAL2 project at GANIL [10], by a collaboration that largely coincides with that involved in the ACTAR JRA. The LoI received a positive review from the SPIRAL2 Advisory Committee.

Very recently, ACTAR has eventually been included in the FP7 SPIRAL2 Preparatory Phase project [11], alongside the other new instrumentation proposed for SPIRAL2. This framework will allow continuing the R&D work, exploiting and improving

on the knowledge built during the JRA. Another goal is to arrive at the signature of an MoU for the construction of the detector.

These developments are giving us the opportunity of re-launching and consolidating the collaboration around ACTAR, also including new partners like ISOLDE (CERN). This goes into the direction of building a device to be used at various facilities, in order to exploit at best the possibilities offered by the instrument in conjunction with the ongoing radioactive ion beam developments.

2 Detector concept

2.1 Detection principle

The ACTAR detector uses the principle of a time-projection chamber (TPC) [12]. The latter is a gaseous detector, capable of tracking in three dimensions the charged particles traversing its volume.

The working principle is illustrated in Fig. 1. In a TPC, electrons are produced by the ionization of the atoms of the gas, induced by the energetic charged particles. An electric field causes the electrons to drift to an amplification zone, where their number is multiplied (with *gain factors* ranging from 10^3 to 10^6). Different technologies can be used to achieve the amplification. The electrons cause a signal (either by induction, or by direct collection) on a segmented plane, creating a two-dimensional projection of the ionization track. The third dimension is reconstructed by measuring the drift time of the electrons through the gas volume.

In the active target mode (see Fig. 2), the events of interest are those in which the incoming beam nuclei interact with the nuclei of the gas atoms. From the detection of the tracks, the reaction vertex can be directly reconstructed. This allows using a very large target thickness, with an increase in luminosity of a factor 5 to 10 with respect to solid targets, without losing in energy resolution. The energy of the particles can be estimated from the amplitude of the signals collected along the whole track; for particles that escape the gas volume, ancillary charged-particle detectors can be placed to intercept them. In any case, information about the specific energy loss is available: by combining such information with that related to the kinematics of the process, identification of the particles can be achieved. In fact, for an identified particle stopping in the gas volume, a more accurate energy measurement is provided by the length of the track (range).

Besides reactions, the detector can be used to measure charged particles (ions) emitted in the decay of unstable nuclei. In this case, a beam of such nuclei is stopped in the detector volume, where the subsequent decay is recorded. Due to the very different specific energy loss, ion emission is easily identified.

The choice of the gas and its pressure is set according to the physics case of interest. For the pressure in particular, the requirements in terms of total target thickness and range for the particles of interest have to be taken into account; for a decay measurement, the pressure is such that the beam is stopped within the detector. In practice however, the gas also has to ensure the good operation of the detector, responding to several factors [13]: low working voltage, high gain, good proportionality and high rate capability. In a number of reactions or decay studies, gas mixtures are employed to reach higher drift velocities or gains.

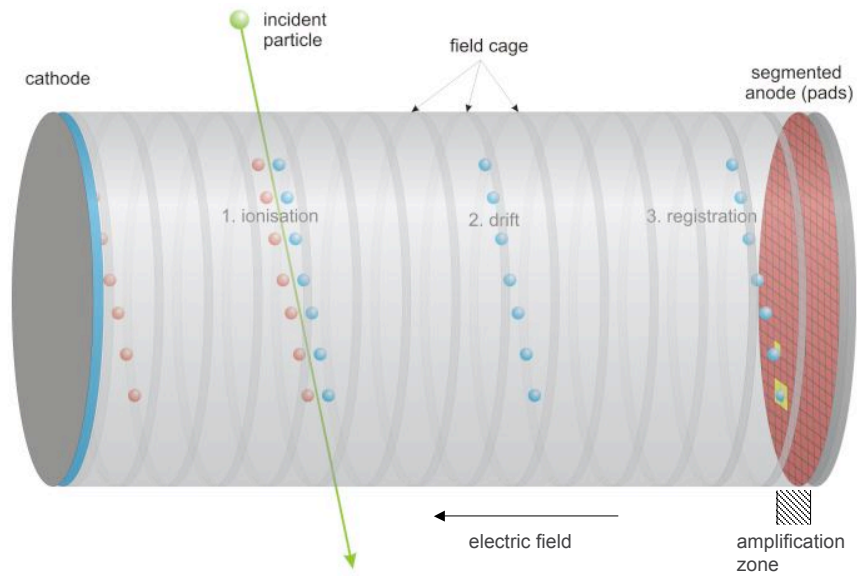


Figure 1: Working principle of a time-projection chamber.

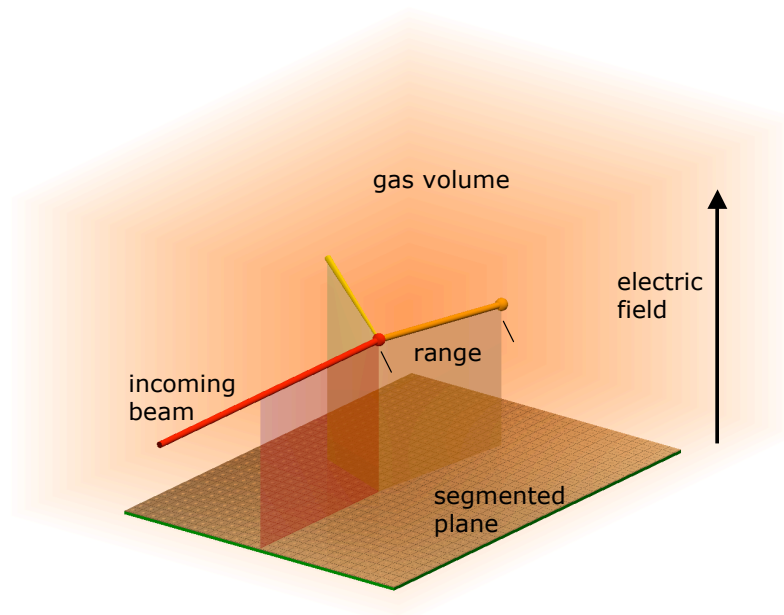


Figure 2: Arrangement of an active target detector.

2.2 Present active target detectors

The validity of the TPC concept, and in particular active targets, in low-energy nuclear physics has been proven by the important results obtained in several experiments employing such devices.

IKAR The archetype of these instruments is IKAR, a hydrogen-filled chamber used to measure elastic scattering of light exotic nuclei on protons in inverse kinematics [14–16]. IKAR is operated at a pressure of 10 bar with the high-energy beams from the GSI fragmentation facility. Results on nuclear matter distributions of ${}^6,8\text{He}$, ${}^{8,9,11}\text{Li}$ and lately on ${}^{12,14}\text{Be}$ and ${}^8\text{B}$ were obtained in the recent years.

MAYA For the lower energy range, the MAYA detector was developed at GANIL [17]. In MAYA, anode wires are used for the amplification, and induced charges are collected on a plane (in this case a cathode) segmented into 32×32 hexagonal pads of about 0.8 cm size. The drift time is measured from the signals on the wires (with respect to an external beam detector which provides the trigger). The wires are arranged parallel to the beam direction, so that the signals of two traces projecting on opposite sides of the centre are collected on different wires. The readout of the pads is performed with the GASSIPLEX chips [18]. MAYA has been successfully used in a variety of conditions:

- A resonance state in the ${}^7\text{H}$ system has been identified via the ${}^{12}\text{C}({}^8\text{He}, {}^7\text{H}){}^{13}\text{N}$ transfer reaction [19, 20], with the ISOL ${}^8\text{He}$ beam from SPIRAL at 15.4 MeV/nucleon. The events of interest were selected by detecting the ${}^{13}\text{N}$ ions in coincidence with tritons (from the breakup of ${}^7\text{H}$), the latter being stopped in an array of CsI scintillators covering the forward angles. The filling gas in this case was isobutane (C_4H_{10}) at a pressure of 30 mbar.
- In a campaign at TRIUMF, the correlation of the two neutrons in the halo of ${}^{11}\text{Li}$ halo nucleus was studied via the ${}^1\text{H}({}^{11}\text{Li}, {}^9\text{Li}){}^3\text{H}$ transfer reaction at 3 MeV/nucleon beam energy [21]. All the outgoing particles were detected in the C_4H_{10} gas at about 100 mbar pressure and, in some cases, stopped in solid-state detectors placed at forward angles. From the Q -value of the reaction, also performed at a different beam energy and at a gas pressure at 350 mbar, the mass of ${}^{11}\text{Li}$ was re-measured as well [22].
- A 50 MeV/nucleon ${}^{56}\text{Ni}$ beam produced by fragmentation and in-flight separation at GANIL was used to measure the inelastic scattering on deuterons in inverse kinematics, with the aim of populating the giant monopole resonance [23]. The position of the resonance is related to the nuclear matter incompressibility. MAYA was operated with deuterium (D_2) at a pressure of 1050 mbar, equivalent to a CD_2 target of 6.3 mg/cm^2 , and tuned to optimize the detection of the scattered deuterons. To avoid saturation from the strong signals induced by the incoming beam, the latter was shielded with two plates placed above and below

the beam trajectory. A similar experiment, this time with a ^{68}Ni beam, has been already approved at GANIL.

CENBG TPC The group at Bordeaux-Gradignan developed a time-projection chamber [24] for the study of two-proton radioactivity. The proton-emitter nuclei are implanted in the centre of the active TPC volume, where the decay takes place. The electrons produced by the implanted nuclei and by the protons emitted in the decay drift towards the amplification zone, which is constituted by a set of four Gas Electron Multipliers (GEMs) [25]. The electrons are then collected on a plane (this time an anode), segmented in two sets of $384 + 384$ orthogonal strips with a pitch of $200\ \mu\text{m}$. The system was recently used for the study of two-proton emission from ^{45}Fe [26] with an in-flight separated beam produced at GANIL. The two protons were clearly identified by measuring their individual energies and their relative emission angle, which are the quantities required to study the emission dynamics of two-proton radioactivity. The gas used was a mixture of 90% argon and 10% methane (CH_4).

Although successful in the measurements listed above, the present TPCs for low-energy nuclear studies have characteristics that limit significantly the physics potential of such instruments. For reaction studies:

- The *dynamic range* is limited: because of the very different specific energy loss for particles of different charge, it is in most cases very difficult to select conditions that would allow detecting at the same time the incident ion, the ejectile and the recoil particles. This is probably the main limitation in MAYA at present.
- The physics cases are limited to two-body reactions, because the time measurement does not allow dealing with multi-hit events.
- The angular coverage is limited in practice to ± 45 degrees relative to the pad plane because of the uncertainties in the reconstruction of “steeper” trajectories from their short projections, thus halving the potential yield and statistics.
- With the present electronics, the achievable number of channels of such a set-up is at maximum about 1000. This forces the use of large pad sizes and hence a lack of energy and angular resolution.
- The lack in position resolution induces an uncertainty on range measurements and thus on the identification of particles in mass and charge.
- The rate of accepted events is limited due to the capabilities of the data acquisition system in terms of through-put.

Limitations of the present arrangement of the TPC for decay studies include the following:

- Due to the use of strips instead of pads, only two particles can be observed in one event. ^{45}Fe also has also a three-proton decay branch which is difficult to identify with this set-up.
- Also, the use of strips instead of pads creates ambiguities in the reconstruction process for certain event geometries.
- Only one time stamp, and not the time evolution of the signal, is available for each strip, which limits the separation of two protons for events where the two protons overlay in the two-dimensional projection.
- The energy resolution for the protons depends on the position resolution which in turn is limited by the charge spread due to the GEMs.
- The size of the chamber is limited by the number of electronic channels which can be handled by the data acquisition system.
- Two-proton emitters have short half-lives (ms) and the data acquisition dead time after the detection of the mother nucleus leads to losses of the radioactivity events.

These problems are addressed in the development of the new detector ACTAR.

Other active target detectors are being developed by various laboratories. Besides the instruments listed in section 1.2, involved in the development of the GET electronics, we mention the TACTIC chamber [27, 28] for nuclear astrophysics (York, TRIUMF); the gas proportional counter of the ANASEN array [29] (Louisiana State University and Florida State University); a TPC for fission studies [30] (Lawrence Livermore National Laboratory).

2.3 ACTAR description and performances

ACTAR will retain the versatility shown by MAYA. Since it will be used with low-energy, heavier ion beams that will become available for reaction studies at ISOL facilities, a better energy and position resolution than MAYA will be necessary.

The final list of specifications of ACTAR will be formulated in the course of the project; one specific activity is dedicated to this purpose (see section 6.1.1). Nonetheless, the work carried out during the ACTAR JRA has identified some key physics cases, which determine a number of performances required from the active target. The physics cases are discussed further in the document, in section 4. The preliminary list of performances is presented in Table 1.

Various elements of the detection setup play a role in several of the parameters, as indicated in the Table. In the following, the complex interplay is discussed in detail, providing a functional description of the ensemble. The systematic description of the detector parts will be presented in section 5.

Table 1: Summary of the performances of ACTAR.

Parameter	Value	Depends upon
Dynamic range	10^3	<ul style="list-style-type: none"> - amplification technology - detector geometry - electronics - ancillary detectors
Number of tracks	all tracks detected independently	<ul style="list-style-type: none"> - segmentation using pads - electronics
Spatial resolution	< 2 mm	<ul style="list-style-type: none"> - amplification technology - pad size and shape - number of channels - ancillary detectors
Maximum beam intensity	10^6 pps	<ul style="list-style-type: none"> - drift velocity - operating conditions (gas type or mixture) - detector size - electronics
Timing resolution	20 ns	<ul style="list-style-type: none"> - drift velocity - electronics
Energy resolution (signal amplitude)	2%	<ul style="list-style-type: none"> - spatial resolution - operating conditions - amplification technology
Efficiency	$> 90\%$	<ul style="list-style-type: none"> - dynamic range - detector geometry - type of event
Counting rate for accepted events	1 kHz	<ul style="list-style-type: none"> - electronics - pad-to-electronics topology
Minimum half life decay events	≈ 10 μ s	<ul style="list-style-type: none"> - electronics
Portability		<ul style="list-style-type: none"> - detector design - electronics

- *Dynamic range* It is the ratio between the largest and smallest charges detectable in the gas volume. From the specific energy loss for different particles in the processes of interest (see also appendix A), we see that a factor 10^3 is required. In most cases, the largest ratios occur between beam or beam-like particles and light recoils, with the former concentrated on a path in the central zone of the detector. In this case, results can be achieved by using an *amplification technology* and electronic slow-control versatility capable of producing different gains on different areas of the segmented plane and for various events, with a lower gain in correspondence of the projection of the beam tracks. Various solutions are presently at study (see section 5.4).

The detector will be designed to be adjustable electromechanically so that the *geometry* of the detection can be modified. For example when the detection of the beam particles is of no interest, the segmented plane can be oriented perpendicularly to the beam direction. This solution minimizes the area of the plane which is “blind” due to the projection of the beam tracks.

For particles differing significantly in charge, outside the beam path, the main aid will come from the newly-designed *electronic system* (GET, General Electronics for TPCs, section 5.8), which will have an intrinsic dynamic range of a few hundreds.

In some cases, even at high pressures, energetic light particles will escape the gas volume. The use of charged-particle *ancillary detectors* becomes then necessary to recover the full energy. However the position information could still be provided from the signals within ACTAR, relaxing the requirements on the ancillary detectors in terms of segmentation.

- *Multiple tracks* Recording more than two tracks, preserving the three-dimensional information, implies collecting the timing signals directly from each point of the projected tracks in an independent way. This forces the choice of *pads* (as opposed to strips) for the segmented plane, and requires an *electronic system* capable of handling the information. Eventually, the limit for the identification of separate tracks should be determined by the spatial resolution.
- *Spatial resolution* The spatial resolution in MAYA is better than the pad size, because the induction created by an electron avalanche on the wires spreads on several pads, allowing a fit for the calculation of the centre of the distribution. Because of other constraints, the *amplification technology* in ACTAR will be of the planar type – GEMs [25] or Micromegas [31], see section 5.4 – with a negligible spread of the electron signal. The resolution will then be essentially determined by the *pad size*. The minimum size is eventually limited by the mechanical constraints related to the collection of all the signals from the pads in the small space available. Also, for a given detector size, the *number of electronic channels* increases for a smaller pad size. Using a larger pad size could be compensated by

scaling the detector accordingly, and using a lower pressure; however, this leads to a larger area that *ancillary detectors* may need to cover, with a substantial impact on the cost of the system. A compromise has thus to be reached.

With the present technology a pad size of $4 \times 4 \text{ mm}^2$ is certainly feasible; still, new connector solutions are being investigated to go to even smaller values, possibly to $2 \times 2 \text{ mm}^2$. Possibilities to improve the spatial resolution beyond the limit imposed by the pad size include adding a resistive layer on the pad plane to spread the collected charge, or a design of the *pad shape* to relate the information about the energy collected in each pad with the position of the signal on the pad (see section 5.5).

- *Beam intensity* ACTAR is designed to allow performing experiments with the most exotic radioactive beams, at intensities as low as 10^3 pps. In some cases however, for processes with a very low cross section, the use of higher beam intensities is desirable. We fix the limit at 10^6 pps, which would allow measurements of exotic giant resonances, and give access to interesting cases in nuclear astrophysics. The allowed beam rate sets a constraint on the minimum *drift velocity* v_d of the electrons, which in turn depends upon the *filling gas* and *applied voltage*. The size of the detector also plays a role: to evacuate the electrons from a chamber of about 40 cm in the direction of the field, before the following beam particle arrives, a drift velocity $v_d = 40 \text{ cm}/\mu\text{s}$ is necessary. This is a very high value, but it can be substantially relaxed by using a *multi-level triggering system* with pattern recognition capabilities, which would identify an event of interest and subsequently block the collection of signals from the beam area. Typical conditions for TPCs can then be used, with $v_d \approx 5 \text{ cm}/\mu\text{s}$ or less.
- *Timing resolution* The timing resolution determines the spatial resolution in the direction parallel to the electron drift, via the value of the *drift velocity*. It should be such, to match the spatial resolution in the other two directions. For $v_d \approx 5 \text{ cm}/\mu\text{s}$, the required timing resolution is 20 ns. The information (evolution of the charge signal) is collected on the pads, and the GET electronic system will provide a numeric signal registration from which a precise time measure can be extracted.
- *Energy resolution* For particles stopped within the gas volume, the energy information is extracted from the range, and thus the error depends on the *spatial resolution*. The absolute values vary with the particle nature and energy, see appendix A.

More in general, the energy deposited in the detector is measured from the amplitude of the signals collected on the pads. Achieving a good resolution, uniform on all the pads, can be extremely challenging in a gas detector: the gas should be operated in the best “proportional” conditions (accurately choosing the *gas*

mixture, its *pressure* and the *applied voltage*), but certainly a key factor is the choice of the *amplification technology*. In this respect, a planar solution (GEMs or Micromegas) is preferable. Recently, tests for the NEXT detector (a TPC for neutrinoless double beta-decay [32]) have shown that, using Micromegas, an intrinsic resolution of less than 1% for α particles from a standard source can be achieved.

- *Efficiency* It is related to the *dynamic range* and the possibility of “using” the events with tracks which lie at small angles with respect to the field direction, thus having short projections and close to the beam. It is possible to act on the various parameters influencing the *track lengths* and on the *geometry* of the detector (for example by orienting the beam perpendicular to the pad plane, see section 5.5), in order to optimize the detection efficiency *for the events of interest*. The goal is to reach at least 90%.
- *Counting rates (accepted events)* This limit is essentially determined by the performance of the *electronics and data acquisition system*. The GET system (section 5.8) is designed to achieve 1 kHz for accepted events, and to have a multi-level triggering system which will be capable of selecting the events of interest by taking into account coincidence signals from external detectors, the pad multiplicity and the hit pattern. Attention needs to be put in the way the pads are grouped with respect to the front-end electronic cards that perform the fast event analysis (*pad-to-electronics topology*).
- *Decay detection* Nuclei showing an interesting decay pattern are often those close to the driplines, with very short half lives. The decay takes place very shortly after an implantation, thus it is important that the dead time of the *acquisition system* be as short as possible. Again, the GET electronics is explicitly taking this aspect into account, operating in an almost “continuous” acquisition mode between an implantation event and the subsequent decay.
- *Portability* We intend to build a portable device to exploit the possibilities offered at the various radioactive ion beam facilities in Europe and possibly elsewhere. This has an impact in the *design of the detector*: we chose for a configuration which does not include a magnetic field – which could serve to confine the particles within the gas volume. Instead, we will utilize ancillary charged-particle detectors placed in order to optimize the dynamic range for the events of interest. As a consequence, the detector will be rather compact, within the constraints imposed by the mechanics of the pads readout. In addition, the GET *electronics* is designed to reach a high level of portability and integration with several types of ancillary detectors through the incorporation of a time-stamping event building.

The considerations made above show that the dimensions of the detection volume in ACTAR strongly depends on the size of the pads. For an ideal size of $2 \times 2 \text{ mm}^2$, the detection volume could be about 30 liters. In this case (but also for a slightly larger pad size) the number of pads is very large, of the order of 20000. Clearly the development of the GET dedicated electronics is necessary to handle all the information.

GET is also designed to be scalable, flexible and with a a number of features that can be adjusted, in order to optimize its performances according to the needs of the specific measurement. The variety of operating conditions for the different physics cases suggests in fact that ACTAR as a whole should be built as a detector with a *variable configuration*. Through the ACTAR program two principle configurations topologies were studied, with the field parallel (axial configuration) and perpendicular (planar configuration) to the beam direction. It was shown that the optimal geometry depends on the reaction under study. The cost of building the field cage and the associated amplification modules corresponds to only a few percent of the total costs, opening this possibility of a flexible design.

3 Physics motivation

3.1 Opportunities with Radioactive Ion Beams

The first category of physics cases for the active target can be characterized under the general denomination of direct and resonant reactions induced by radioactive beams. Forty years ago, stable nuclei were studied in direct kinematics with beams of light ions, and a wealth of nuclear structure information was obtained from direct reaction results. With radioactive beams, these reactions are nowadays studied in inverse kinematics on light target nuclei such as protons, deuterons or α particles because light nuclei are known to be the best probes to extract nuclear structure information. Since all these light nuclei are gases, they can be used as detection gases in active targets.

Reactions of interest include elastic and inelastic scattering; transfer of one, two, or few nucleons; resonant reactions where states in the compound nucleus are investigated. In the following sections we present these cases and discuss the use of the active target method.

Another application where these detectors present interesting features is the study of exotic radioactivities, such as two- and three-proton radioactivity, which require the precise determination of the energy and angle of the individual protons; or β -delayed multi-particle emission, where the nature and correlation of the emitted ions is of interest. The gas detector is in this case used as a time-projection chamber and not as an active target *stricto sensu*, since the gas only acts as stopping medium for the nuclei of interest, however the technical requirements are very similar to those of an active target.

From the above list, it is clear that the physics cases considered for the active target cover a very broad range of nuclei, from light halo nuclei up to the relatively heavy beams which will be available from SPIRAL2. The energy range also goes from the lowest energies of an ISOL post-accelerated facility for resonant reactions studies up to several tens or hundreds of MeV/nucleon of the in-flight facilities for matter density determination, giant resonance studies and proton radioactivity. Active targets have the possibility of exploiting all these regimes, as already shown by the results obtained with the present devices.

3.2 Elastic scattering

The simplest of all reactions, elastic scattering, is used at high energy (few hundreds MeV/nucleon) to study matter density distributions. A complete experimental program is dedicated to this subject at GSI with the IKAR active target, and has produced many impressive results on the matter density distributions of halo nuclei [15, 33, 34]. At lower energy, elastic scattering is often the first reaction to be studied, because the cross sections are high, and also because it allows to determine the parameters of the

optical potential which is needed to analyse inelastic scattering and transfer reaction data.

3.3 Spectroscopic studies with inelastic scattering and transfer reactions

The second type of experiments where active targets can have a large variety of applications is structure studies of very exotic nuclei from inelastic or transfer reactions.

Proton inelastic scattering can yield important information on the structure of nuclei, in particular on transition densities. Protons interact with both protons and neutrons in the nucleus, whereas Coulomb excitation on a heavy partner or lifetime measurements probe directly only the proton density distributions. The combination of the two types of measurements can disentangle proton and neutron contribution to excited states [35, 36]. Another possible use of inelastic scattering is to study giant resonances, in particular the giant monopole resonance, as detailed in section 3.5.

One-nucleon transfer reactions are particularly useful as a spectroscopic tool due to their selectivity in favour of the population of single-particle (or hole) levels. The application of such reactions to exotic nuclei is a major tool to explore the evolution of the shell structure with isospin. The excitation energies of the different states in the nucleus under study can be obtained directly from the measured energy spectra. The Q -values measured for the ground state in these spectra sometimes provide the first determination of the mass in the case of very exotic nuclei, at the limit of drip lines or even beyond [19]. While the angular distributions of the differential cross sections depend on the transferred angular momentum, and therefore bring information on the spin and parity of the state, the absolute values of these cross sections are directly related to the spectroscopic factors and therefore to the structure of the states. Major results have already been obtained, in particular from (d,p) reactions [37]. Other reactions such as (p,d), (d,t) or (d, ^3He) are also considered to study neutron hole or proton hole states, respectively.

Many regions of the nuclear chart are of particular interest for transfer reaction studies. The light nuclei, where the drip lines are accessible and where many exotic properties have been evidenced, such as one-neutron and two-neutron halos, or borromean structures, have already been studied extensively but many experiments suffered from the lack of statistics which prevented to draw firm conclusions. The availability of higher intensities in the next-generation facilities will help to shed some light on several controversial results in systems such as $^5,7\text{H}$ or $^7,9\text{He}$. The change of shell structure in regions far from the valley of stability has opened a new challenge to our traditional models of the nucleus. Some of the conventional shell gaps have been quenched in extreme neutron-rich regions while new ones have surfaced up. A complete understanding on the evolution of nuclear orbitals over the nuclear chart is therefore now an important task. The nuclei far from stability corresponding to both the traditional magic

numbers and to the predicted new ones, are of course the focus of transfer reaction experiments. The new regions of nuclei that will become accessible with SPIRAL2 with unprecedented intensities are a strong motivation for the development of new generation detection devices such as ACTAR.

Finally, transfer reactions are also an important tool for nuclear astrophysics experiments. Despite recent improvements in detection systems, the direct study of some astrophysically important reactions is simply not feasible at the relevant energies and thus indirect techniques must be exploited. However, many of the reaction rates under investigation are dominated, at astrophysical temperatures, by the contribution from one or two resonances, and so information on the properties of these resonances (energy, spin and width) allows the contribution to the total reaction rate to be calculated. Transfer reactions, such as (d,p) and ($^3\text{He,t}$), are powerful tools for investigating these properties for key energy levels in the relevant nuclide.

In general transfer reaction experiments use a sophisticated set-up which consists of a spectrometer to detect the projectile residue, an array of solid state detectors such as TIARA [38] or MUST2 [39] to detect the light target recoil, and a gamma spectrometer to detect in coincidence the de-excitation γ rays. This is needed when the nucleus under study has a high density of excited states, where γ -ray detection is the only way to obtain the needed resolution. Moreover, the target thickness is limited due to the very low energy of the recoil nucleus. As a consequence, this type of detection set-up requires reasonable beam intensities, of the order of a few 10^4 - 10^5 pps at minimum. The advantage of active targets in this kind of studies lies in the possibility of using high pressures and thus having a very large target thickness, that allows performing precise measurements already with beam intensities as low as 10^3 . There exists therefore a niche for active target experiments with the most exotic nuclei where incident intensities are too low, or when the recoil nucleus has such a low energy that it cannot exit from a solid target without drastically destroying the energy resolution. Schematically, such active targets will increase the sensitivity by two orders of magnitude with respect to pure Si devices such as MUST2, therefore allowing to reach nuclei with two nucleons further away from stability.

3.4 Resonant reactions

Resonance reactions allow for the production and observation of particle-unstable isotopes, or highly-excited unbound states in nuclei. In both cases, the reaction is performed in inverse kinematics and the states of interest are populated by the resonant capture of a (light) target nucleus onto the incident nucleus. The nuclear state which is created decays after a very short half-life, depending on its decay width. The measurement of the decay channels allows the deduction of spectroscopic information on the nuclear state populated, its energy, its spin and parity, and other characteristics.

When one particular state is studied, the beam energy is chosen in order to cover

the corresponding centre of mass energy when the beam is degraded through the target, usually a CH_2 foil in case of a reaction on protons. In this case the light particles corresponding to the various decay channels escape the target and are detected in the forward direction. Alternatively, an excitation function on a broader range can be obtained by using a very thick target – a gas target is preferred in this case in order to avoid degradation of the light-particle energy. A gas target is also necessary when studying resonant reactions on α particles.

Among the exit channels, elastic scattering has the advantage of having by far the largest cross section. Resonant scattering on protons with a neutron-rich ${}^A Z$ nucleus can be used to populate the Isobaric Analogue States (IAS) of the ${}^{A+1} Z$ nucleus and deduce information on their structure [40], complementing the (d,p) reaction method. Resonant scattering on α particles are used to study states that present pronounced molecular structures [41]. More in general, resonant reactions are particularly interesting for nuclear astrophysics, for which many processes of interest proceed through resonance states. A precise knowledge of the structure of such states can be obtained through the measurements of the various decay channels (elastic, inelastic, other particle-emission channels) after population with reaction on protons or α particles.

Such studies have been performed up to now using conventional set-ups with solid state detectors (sometimes placed within the volume of the target gas [42, 43]). These types of experiments will strongly benefit from the use of active targets, because of the possibility of improving resolution by the determination of the position of the reaction vertex. Several groups are already using such devices [44] or are presently constructing new active target devices for that purpose [27–29].

3.5 Inelastic scattering and isoscalar giant resonances

The study of the compression modes, the isoscalar giant monopole (ISGMR) and dipole (ISGDR) resonances, in stable nuclei has been pursued for the last three decades with the aim to determine the incompressibility of nuclear matter [45]. This fundamental property of nuclear matter is of crucial importance. It determines the excitation energies of the compression modes and, as an important parameter of the equation of state (EOS), it plays a crucial role in nuclear collisions and in the outcome of the collapse of heavy stars in what is known as supernova explosions. Through these extensive experimental and theoretical studies, it is now accepted that the incompressibility of nuclear matter K_∞ has a value of around 230 MeV. The asymmetry term in the expansion of the nucleus incompressibility K_τ has been poorly determined, since it requires studies of the compression modes in an isotopic chain spanning a wide range of $\delta = [(N - Z)/A]$ values. This has been done recently for the stable Sn nuclei and a value of $K_\tau = (-550 \pm 100)$ MeV was obtained [46].

With the availability of exotic neutron-rich and proton-rich nuclei, it becomes possible to cover a wider range in δ -values allowing a more accurate determination of

K_τ and also of K_∞ , because of the slight dependence of these two parameters when extracting them from a limited set of data. Furthermore, in these exotic nuclei new phenomena emerge, such as pygmy resonances that are multipole strengths reflecting the collectivity due to the extra neutron-skin or proton-skin relative to the core.

The study of giant resonances in unstable nuclei is quite involved experimentally and has up until recently been restricted to the study of isovector giant dipole resonance (IVGDR) in a number of nuclei at GSI [47, 48] and RIKEN [49]. Recently Monrozeau et al. measured the ISGMR and giant quadrupole resonance (GQR) in the exotic ^{56}Ni nucleus [23] using MAYA. The centroid of the ISGMR was determined with an uncertainty of 0.5 MeV.

The measurement relied on the detection of the recoil deuterons from the inelastic scattering of the beam particles on the D_2 gas in MAYA; the uncertainty of the result is related to the difficult measurement of the range of the deuterons. A significant improvement could be obtained with the use of ACTAR, since a more precise determination of the reaction vertex and track lengths would be possible; and the use of He as a gas would bring an increase of the cross section. This case is examined in section 4.3.

3.6 Exotic decay modes at the driplines

Exotic decays like two-proton radioactivity or β -delayed multi-particle emission are sensitive probes to study nuclear structure at the limits on nuclear stability. Often these decays are the only means to access information this far from stability. In addition, these decays or their reverse, i.e. the capture of particles are of prime importance in astrophysics.

Two-proton radioactivity is supposed to give access to basic information like proton-proton pairing in nuclei, but also on final-state proton-proton interactions [4]. Detailed theoretical models reproducing the experimental results will also allow to determine the composition of the wave function of the emitting nucleus in terms of the orbitals contributing to the decay and the mixing of the different spin contributions (“ j -content” of the wave function). In certain cases, the tunneling process might also be studied while the deformation changes between the parent and the daughter nucleus, a particularly challenging task. Two-proton capture, the reverse process of two-proton radioactivity is discussed as a possible bridge to overcome the slowing-down of the astrophysical rp -process at waiting points like ^{68}Se or ^{72}Kr [50].

Studies of exotic decays like two-proton radioactivity or β -delayed multi-particle emission is usually performed at fragmentation facilities like GANIL/LISE, GSI/FRS, MSU/A1900 or in the future at RIKEN/BigRIPS or FAIR/SuperFRS where the most exotic nuclei are produced in the most efficient way. Such studies cannot be done with silicon detector arrays as it is done for simpler decays, because the different particles emitted in these decays cannot be resolved due to their range.

As the particles cannot escape from the detectors, only the total decay energy, the

half-life and the branching ratios can be accessed. However, to measure e.g. the energy sharing of the different particles or their relative emission angle, which are the observables which allow studying the decay dynamics and to perform detailed comparisons with theoretical models; or in order to distinguish between single-particle emission and multi-particle emission, the individual particles have to be observed with their energy and their angle. This is only possible with gas detectors allowing to visualize individual particles in three dimensions.

Beyond the measurement of the observables mentioned above, another challenge for the study of two-proton radioactivity is the fact that the two-proton emitters have rather short half-lives of the order of 2-10 ms. This means that the experimental device has to be able to treat the implantation of the emitter and its decay in a very short time, which is at or often beyond the limit of data acquisition systems used today. In order to study these decays without significant losses due to acquisition dead time, the detector itself, the electronics and the data acquisition has to be tailor-made for these applications. Typically, the GANIL data acquisition in its standard implementation loses about 30% of the decay events of ^{45}Fe due to its dead time.

4 Detailed physics cases

In this section we develop a few physics cases in more detail. We intend to show the capabilities of ACTAR in these measurements, also with respect to the performances of present active gas detectors. We mostly consider measurements that have been already attempted or actually performed with the present devices, to point out the improvements that ACTAR could bring. In one occasion, that of reactions with the ^{78}Ni nucleus, we have chosen a case which is representative for similar measurements, that will become possible in that region of the chart of nuclei with the development of the new RIB facilities – in particular SPIRAL2, even if the intensity of ^{78}Ni beam itself may still be too low.

That of ^{78}Ni is also the test case where the simulation work has focused in the past months. Results of detailed event-by event-simulations will be presented for this case. For the other ones, calculations of the performances of ACTAR were made based on the known characteristics of the reaction (kinematics), tabulated values for the energy loss of particles (summarized in appendix A) and the characteristics of the ACTAR detector.

4.1 Transfer reactions on ^{78}Ni

Doubly-magic nuclei have traditionally formed the cornerstones of our understanding of nuclear physics. These nuclei have proton and neutron shells which are completely filled and so they have a particularly simple structure. Their properties and those of their nearest neighbours have constrained key ingredients of nuclear structure theories, such as single-particle energies and effective interactions. Doubly-magic nuclei are also essential to be used as the cores for shell-model calculations. This allows the model space to be substantially reduced and makes the shell-model calculations of heavy nuclei feasible. If we consider the classical shell gaps known from studies of stable nuclei, the doubly-magic nucleus with the largest imbalance of neutrons to protons is ^{78}Ni . It is clearly of great interest to establish whether ^{78}Ni is indeed a doubly-magic nucleus and then to study its structure. It therefore represents a crucial testing ground for the structure of very neutron-rich nuclei, where the most unusual nuclear structure is expected to develop. Studies of the single-particle properties and shell structure of nuclei in the region of ^{78}Ni , as well as other doubly-magic nuclei, will thus be needed.

Here we consider an experiment where a ^{78}Ni beam at 8 MeV/nucleon is used to induce transfer reactions on the deuterium atoms of the ACTAR gas at atmospheric pressure. Different reactions can potentially be studied simultaneously, if the different sides of ACTAR are covered with Si-CsI telescopes. Indeed the protons coming from the (d,p) reactions are emitted at backward angles in the laboratory for small centre of mass angles, whereas (d,t) and (d, ^3He) produce tritons and ^3He at forward angles. Finally the deuterons from elastic and inelastic scattering are found close to 90 degrees in the laboratory frame. The missing-mass method is applied to reconstruct the level

scheme of the heavy partner from the kinematical characteristics of the light recoil.

We immediately point out one of the strong advantages of an active target over more classical devices. If a solid target CD_2 is used, to keep a sufficient resolution in the charged-particle spectra its thickness must be below $\approx 500 \mu\text{g}/\text{cm}^2$, and hence $\approx 125 \mu\text{g}/\text{cm}^2$ of D_2 , or 2×10^{19} atoms/ cm^2 . In an active target filled with D_2 at 1 bar pressure, a vertex resolution of 1 mm corresponds to 3×10^{18} atoms/ cm^2 , and hence to a very thin target slice of $\approx 20 \mu\text{g}/\text{cm}^2$. Thus the influence of the energy loss for the final energy resolution is only of about 20/500 with respect to the solid target. Nonetheless, using a detector of 50 cm length, the total thickness will be $\approx 10^{21}$ atoms/ cm^2 ; this is 70 times more than the solid target. This fact, combined with the geometric efficiency, means that lower beam intensities can be used: while in practice solid target experiments for such a reaction are limited to beam intensities above 10^4 pps, with the active target good statistics results were obtained with beams in the range of 100 pps to 1000 pps [21]. This implies that experiments performed with active targets allow studying two isotopes further away from stability as compared to a solid target experiment.

To evaluate the performances of ACTAR for transfer reactions on ^{78}Ni , detailed simulations have been performed using the program ActarSim [51]. The program calculates the ionization (in various possible gases) along the tracks of particles undergoing the reaction of interest, the drift of the electrons in the electric field, their multiplication in the amplification region and the signal collected on the pad plane. Different amplification technologies can be implemented, as well as ancillary charged-particle detectors surrounding the gas volume. For this simulation, the beam was described as having an emittance of 10π mm mrad. The active volume was taken as a cube of 30 cm side; it was filled with deuterium gas at a pressure of 1 atm (1013 mbar) and room temperature. The amplification was that of a Micromegas system (see section 5.4) and the anode pads were squares of $4 \times 4 \text{ mm}^2$, located at the bottom of the cube. Si-CsI telescopes were positioned on the left and right sides of the cube, and on the beam entrance side of the chamber, optimizing for the detection of protons from the (d,p) reaction. The arrangement is shown in Fig. 3.

At atmospheric pressure, the incoming beam loses 2 MeV/nucleon between the entrance and exit of the gas volume. The reaction energy has to be deduced from the reconstruction of the vertex. This was systematically performed using the projection of the tracks of the light particles (eliminating a “blind” region around the beam projection); the resolution on the vertex position was defined as the difference between the reconstructed position and the original one, and it was slightly less than 2 mm FWHM (thus less than half the pad size). At the rate of energy loss of the beam this corresponds to 1.2 MeV of uncertainty on the beam energy, which can be completely neglected with respect to the effect on the energy and angles of the outgoing light particles.

We assumed that 4 states were populated in the (d,p) reaction: the ground state, and three excited states at 1 MeV, 2 MeV and 5 MeV respectively. Fig. 4 shows the results of the simulation for the correlation between the range and the scattering angle

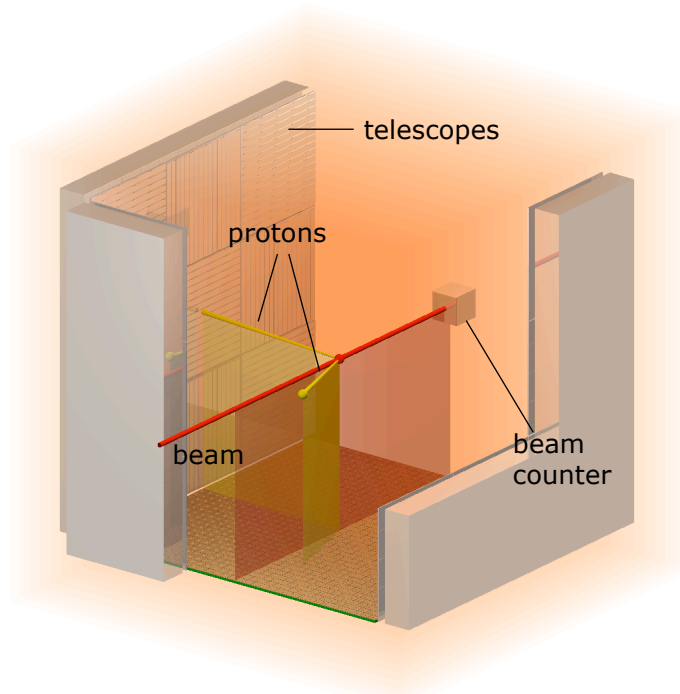


Figure 3: Configuration of ACTAR for the measurement of (d,p) transfer reactions in inverse kinematics. Two proton tracks are shown, one for large angles in the laboratory frame (small centre of mass angles) for which the low-energy proton is stopped in the gas volume; and the second around 90 degrees in the laboratory frame, for which the proton escapes to one of the Si-CsI telescopes (some telescopes have been removed from the view). The beam can be stopped in a counter for normalization and identification purposes; alternatively, ACTAR could be coupled to an external beam detector or spectrometer.

of the recoiling proton, for the different populated states. At large angles, the protons are stopped in the gas volume and the states are clearly separated (see black, red, blue and pink dots at large angles), showing that an energy resolution better than a few hundred keV in the centre of mass frame can be achieved under these conditions. For angles below 120 degrees, the protons have sufficient energy to escape the gas volume: the nearly horizontal lines correspond to the geometric limits of the gas volume. For completeness, the kinematic lines corresponding to elastic, inelastic scattering and (d,t) reactions (excited states at 1 and 3 MeV in both cases) are also shown in Fig. 4. They appear respectively close to 90 degrees and at the most forward angles. In these cases too, the length of the trajectory of the light particle is limited by the geometry of the gas volume. In order to get the full kinematics of these reactions, additional ancillary detectors would be needed at forward angles.

The total energy of the particles hitting the array of Si-CsI telescopes is shown in

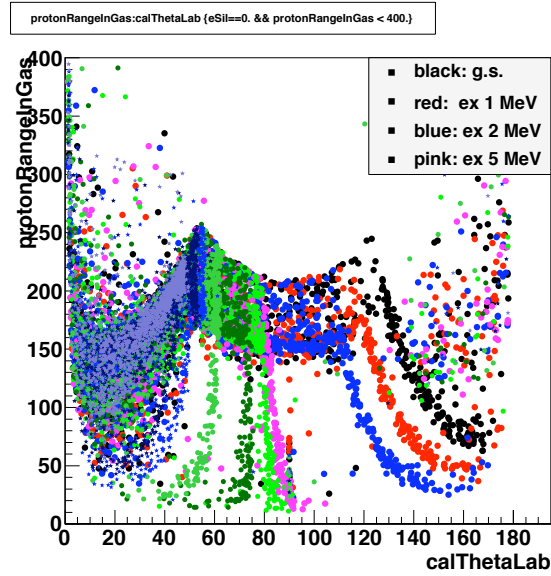


Figure 4: Particle identification for p (black, red, blue and pink dots for transfer to the ground state and states at $E^* = 1, 2$ and 5 MeV respectively); d (light, dark and medium green dots, corresponding to elastic and inelastic to $E^* = 1$ and 3 MeV respectively); and t (stars of different shades of blue for transfer to ground state and excited states at $E^* = 1$ and 3 MeV). The plotted quantities are the length of the particle trajectory in the gas volume versus the laboratory scattering angle.

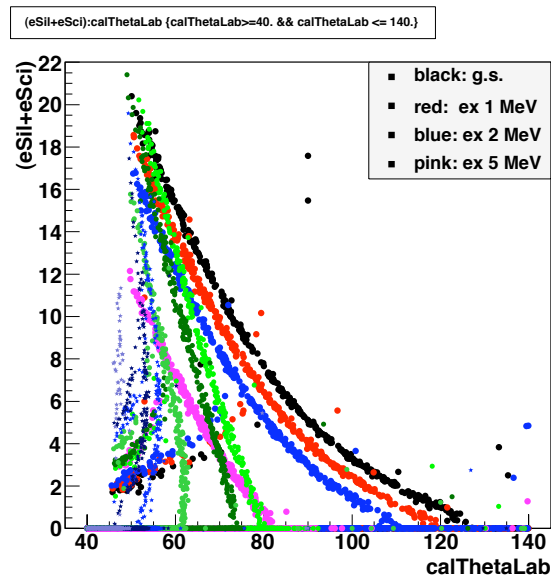


Figure 5: Particle identification for p, d, and t in the Si-CsI telescopes located outside the active gas volume: the detected energy is plotted versus their calculated scattering angle. The colour codes are the same as in Fig. 4.

Fig. 5, where the quantity is plotted as a function of the laboratory scattering angle. The figure shows that a large fraction of the total angular range can be covered with the present geometry, at least for the (d,p) reaction, elastic and inelastic scattering.

In Fig. 4 one can notice that the protons emitted when the 5 MeV excited state is populated in ^{79}Ni (pink dots) do not appear for angles larger than about 90 degrees in the laboratory frame (centre of mass angles lower than 10 degrees). For such angles the proton energy becomes lower than 400 keV, which corresponds to a track length of less than 20 mm which was conservatively set as the minimum range value for which the emission angle and position vertex could be safely determined. Such states at higher excitation energy could be measured by setting a lower pressure to obtain longer tracks and thus the full angular distribution. This was confirmed by simulations run at a pressure of 400 mbar; on the other hand, at that pressure the protons from the transfer to the ground state escape the gas volume at all centre of mass angles.

The geometric efficiency of the ACTAR detector in this configuration and for the various channels is obtained from the simulation. For example for the (d,p) channel at a pressure of 1 atm, the efficiency varies from about 28% of the total solid angle for the transfer to the ground state, to about 22% for the transfer to the state at $E^* = 5$ MeV. To obtain the corresponding yields, one would have to fold in the efficiency, which depends upon the scattering angle, with the angular distributions of the cross section. We can nevertheless make a crude estimate for a constant cross section of 1 mb/sr in the covered range: with a beam intensity of just 10^3 pps, about 10 events/h would be detected for a target slice of 1 cm (corresponding to a range in the centre of mass energy of the scattering of less than 100 keV), i.e about 300 events/h for the whole detector.

The dynamic range required to detect the beam particles together with the light recoil nuclei can be extremely large, because of the very different specific energy loss dE/dx . At a pressure of 1 atm, the beam particles (8 to 6 MeV/nucleon) deposit about 700 keV/mm; protons which are stopped in the gas deposit a little more than 10 keV/mm at the Bragg peak, but more energetic protons may deposit less than 1 keV/mm (0.5 keV/mm at 20 MeV: see Fig. 23 in appendix A). To detect the light ions stopped in the gas volume, also on trajectories close to the beam, the electronic system will ensure a dynamic range of at least 10^2 . For particles escaping the gas volume, the energy will be recorded in ancillary detectors; however, to relax the requirements on the granularity of the latter, it is desirable to detect the tracks of such particles in the gas. For this purpose, the corresponding areas of the pad plane will amplify the electron signal with a higher gain than the area of the beam projection, utilizing the technologies that are described in section 5.5.

These simulations show the performances that can be expected for such type of experiments with beams produced by SPIRAL2 in this energy region, since the kinematics is mainly determined by the mass of the light partner. The necessary intensity for this type of experiment is as low as 10^3 pps.

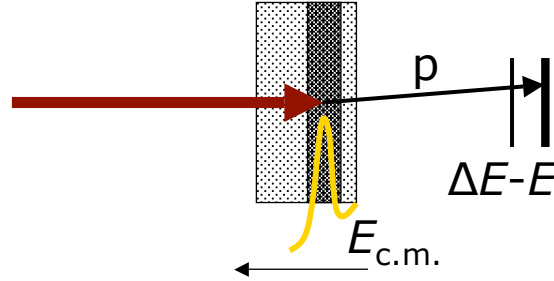


Figure 6: Resonant reactions in a thick target in inverse kinematics: the energy of the beam is degraded through the target, and reactions mainly occur at centre of mass energies corresponding to a resonance. The beam is stopped in the target, while the light recoil escapes and is detected and identified at small angles.

4.2 Resonant reactions: $^{26}\text{Ne}+p$

Resonant reactions are used to gain access to states of the compound nucleus, which lie above the threshold for breakup into the colliding particles. In section 3.4 we mentioned how resonant elastic scattering is a valuable tool for nuclear spectroscopy studies via the population of isobaric analog states (IAS). Here we consider the $^{26}\text{Ne}+p$ resonant scattering to populate the isobaric analogs of states in ^{27}Ne . This nucleus is of interest as the presence of an excited state with negative parity [52, 53] points to the reduction of the $N = 20$ shell gap in this region. A ^{26}Ne beam is available for example at SPIRAL with an intensity of a few 10^3 pps.

In resonant elastic scattering measurements, the beam energy and the target thickness are chosen so that the energy range of the states of interest is covered by degrading the beam through the target (see Fig. 6). The recoiling light particles are detected at forward angles, and the centre of mass energy of the scattering is reconstructed from the kinematics (angle and energy of the light particle). Information about the spin and parity of the state can be obtained from the angular distribution, and also, in some cases, from a fit of the shape of the resonance. Usually a thick target is used to completely stop the incoming beam, so that the light particles can be detected around zero degrees (in the laboratory frame) in a charged-particle telescope. Either a solid target (CH_2 , for proton scattering) or a gas target (for He or proton scattering) can be used. A rather good resolution can be achieved thanks to the inverse kinematics conditions; at 0 degrees (180 degrees in the centre of mass frame), the centre of mass energy $E_{\text{c.m.}}$ at the scattering point (energy of the resonance) is related to the energy of the recoil light particle E_r through the ratio of the masses of the target and projectile:

$$E_{\text{c.m.}} = E_r \frac{m_p + m_t}{4m_p}$$

which reduces to $E_{c.m.} \approx E_r/4$ for proton scattering, with a corresponding reduction of the error. However, the resolution degrades very rapidly with the angle of the recoil particle, and only the events around zero degrees can be used to measure the excitation function.

A problem can occur if the projectile nucleus has low-lying excited states, because inelastic scattering cannot be separated; its contribution is usually neglected. But the most important limit is represented by the small solid angle for the detection of the light particles, which makes it necessary to have rather high beam intensities to perform such measurements. In the case considered here, with a detector covering the forward angles at ± 10 degrees from the beam direction at a distance of about 10 cm from the scattering point, one can calculate that the number of events originating from a resonance width of 100 keV is about 0.3 per hour, for a beam intensity of 10^3 pps and an average cross section through the resonance of 100 mb/sr.

The use of an active target brings two significant advantages to this method. On one side, the position of the reaction vertex can be directly detected from the projection of the tracks on the pad plane or, for scattering at zero degree, by the change in the charge profile on the pads. The resolution in terms of centre of mass energy depends upon the energy loss rate of the beam and thus the gas pressure. In order to stop the beam (^{26}Ne at 3 MeV/nucleon, corresponding to a compound nucleus excitation just above the position of the IAS of the ^{27}Ne ground state) in about 40 cm of gas, a pressure of 50 mbar of isobutane is sufficient; at an energy loss of about 12 MeV/(mg/cm²) (value at the energy of the IAS resonance) this translates into a distance of 20 mm for 100 keV of energy loss. The vertex position is determined by the intersection of the tracks, and its resolution is better than the pad size; we make here a conservative estimate of 1 mm corresponding then to a centre of mass energy resolution of 5 keV; this should be compared to the 30 keV obtained in a similar measurement with a solid target [54]. This configuration, however, would place the IAS (ground state) resonance near the entrance of the chamber, preventing seeing resonances at higher energy; in addition, the recoil protons would have a large range in the low pressure (already 15 cm for an energy of 1 MeV), escaping the gas at all positions around the volume.

A more convenient configuration is that using a higher beam energy and a higher pressure, in order to place the resonance of the ground-state IAS closer to the end of the chamber: for example, at 8 MeV/nucleon and 200 mbar the scattering would take place after at 40 cm from the entrance of the chamber. This allows measuring a more extended excitation function, but especially makes it possible to exploit the second advantage of the active target, which is the determination of the full kinematics: the recoil proton (angle and energy), the vertex position *and* the range of the scattered beam nucleus are measured (the latter is unique to active targets). With this information, the events where the protons are scattered at angles larger than a few degrees can also be used to measure the excitation function without any loss of resolution; and events due to inelastic scattering can be completely separated.

The range of the recoil protons, calculated from their energy after the scattering, is shown in Fig. 7 as function of the scattering angle. The forward scattered protons have energies up to almost 10 MeV, and cannot be stopped in the gas. ACTAR can be arranged as shown in Fig. 8, with ancillary detectors placed in the forward direction. The beam energy and the pressure are tuned so that the recoil protons from the ground-state IAS resonance are either stopped in the ancillary detectors or in the gas volume. With this arrangement the efficiency increases significantly (a few hundreds times) with respect to a solid target. To correctly estimate the gain in yield, a full simulation should be made taking into account the angular dependence of the cross section; but it is already possible to conclude that an improvement of a *factor 50 to 100 in statistics* is achievable, making the measurement feasible with the present SPIRAL ^{26}Ne beam.

Other resonances, higher in energy, are situated in regions closer to the target entrance and produce protons at higher energy, for which the detection efficiency is lower as they may escape through the sides of the gas volume. We observe however that the information about the scattering energy (assuming an elastic scattering) can be reconstructed from the range of the scattered beam nucleus and the angle of the recoil proton.

In this illustration of the performances of ACTAR we have supposed that it is possible to detect at the same time the heavy beam nucleus and the light recoil proton. The energies deposited by the two particles in the gas are very different, as shown in Fig. 23 in appendix A. There is a factor ≈ 500 between the maximum energy deposited by ^{26}Ne and the minimum energy of protons when they recoil in the forward direction at about 10 MeV energy. This factor dictates the dynamic range in ACTAR, as specified in the requirements listed in Table 1. It has to be achieved by a combination of the electronic system GET and other specific solutions for the various cases. Here, one can use a lower amplification on the central area of the pad plane, where the projection of the beam track occurs (the methods are discussed in section 5.4). For the protons diffused close to zero degrees, thus in the beam path, accurate information about the energy and angle can be obtained by using a finely segmented silicon detector covering a few square centimeters. For larger angles the proton recoil out of the beam path and their direction can be measured in the gas volume; the ancillary detectors in the forward direction would complete the information on the energy, but they do not need to be highly segmented.

4.3 Inelastic scattering and GRs: $^{56}\text{Ni}(\alpha, \alpha')$

The measurement of this type of reaction has already been performed using MAYA [23], with a ^{56}Ni beam at 50 MeV/nucleon, delivered by GANIL, and deuterium as detection gas and target nucleus. The available beam intensity was 10^6 pps, but MAYA could only accept 5×10^4 . From the detection of the inelastically scattered deuterons (angle and energy, the latter deduced from the range of the deuterons), the

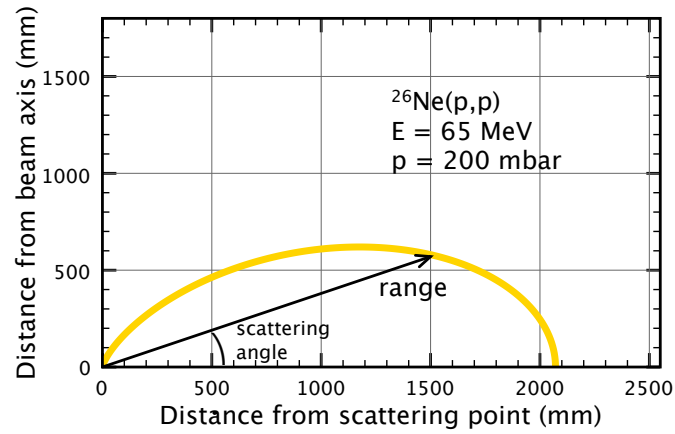


Figure 7: Range of protons recoiling from the elastic scattering with a ^{26}Ne projectile nucleus at an energy of 65 MeV, corresponding in the compound nucleus to the IAS of the ground state of ^{27}Ne . The energy loss calculations have been performed using SRIM [55].

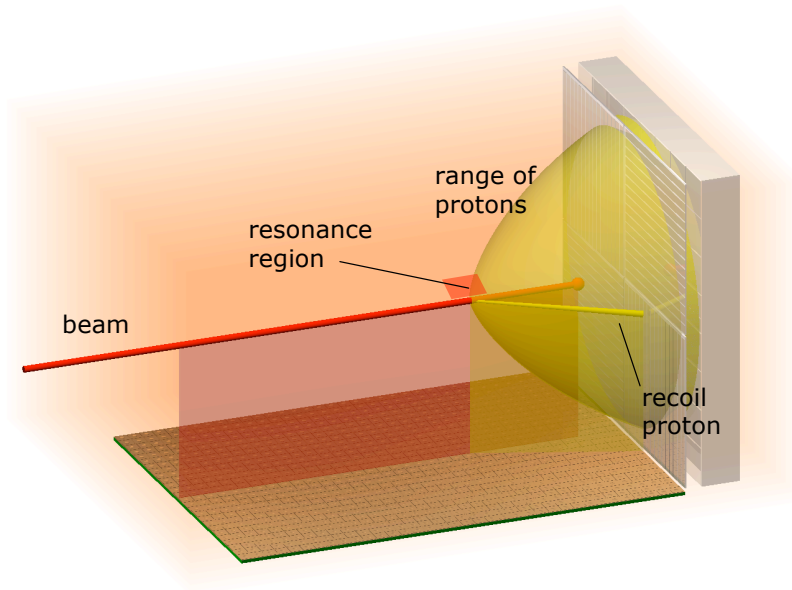


Figure 8: Configuration of ACTAR for the measurement of resonant reactions. Ancillary detectors are placed at forward angles to intercept charged particles escaping the gas volume. The range of protons is calculated from their energy after the scattering (see Fig. 7).

giant monopole (GMR) and giant quadrupole resonances (GQR) in the excitation spectrum of ^{56}Ni were observed with a resolution of a few MeV. In order to detect the small signals of the deuterons, the beam was shielded with two plates above and below its path, to prevent the electrons created by the beam particles from reaching the amplification wires. As a consequence, part of each deuteron track was lost; and the vertex of the reaction could not be measured with great accuracy.

With ACTAR the study of this reaction could advance further, with improvements both in efficiency and resolution. The measurement of the isoscalar giant dipole resonance (ISGDR), situated higher in excitation energy at about 30 MeV in ^{56}Ni , would also become feasible; and the microscopic structure of the GRs could be investigated by detecting the protons emitted in the decay [56].

As detection gas we consider a mixture of He and CF_4 . Helium is a better target nucleus than deuterons for these reactions, as it ensures a larger cross section and less background from other reaction channels (for example deuteron breakup). CF_4 is added as a quenching gas, allowing to operate the amplification stage at a tension high enough to have the necessary gain, without incurring in discharges; our recent tests showed that 5% of CF_4 is sufficient.

The gas pressure should be set high in order to have the largest possible target thickness; at the same time the range of the recoil α particles should be long enough to ensure a good resolution in the determination of their energy. In addition, the detection of the α 's should be covered for angles up to about 10 degrees in the centre of mass system, to allow performing a fit of the angular distribution and thus identify the GR mode [57]. Notice that the beam particles do not play a role in the choice of the gas pressure, because they only lose a fraction of their energy traversing the whole target.

Fig. 9 shows, for a given scattering point placed at the origin of the diagrams, the loci of the α particles stopped in the gas (He + 5% CF_4 at 1 bar pressure); elastic and inelastic scattering with Q -values from -25 to -35 MeV are shown (the width of the ISGDR is expected to be about 5 MeV [58]). The left panel shows that, at this pressure, α particles with a centre of mass scattering angle up to 10 degrees are certainly stopped in the gas volume; the right panel is an enlargement close to the scattering point, that shows the resolution that can be achieved with ACTAR. The grid reproduces the maximum expected size of the pads of ACTAR, $4 \times 4 \text{ mm}^2$; a position resolution of 2 mm on the determination of the range corresponds to about 1.5 MeV resolution on the Q -value of the reaction — or excitation energy of the ^{56}Ni projectile. We can see that for this physics case, a very good position resolution is crucial; in any case, it is not useful to increase the pressure beyond 2 bar at maximum. The angular resolution, on the other hand, is better than one degree in the centre of mass system. This is important, because it allows a fit of the angular distribution, which can help disentangling the various GR modes. A calculation of expected cross sections for exciting GRs is shown in Fig. 10 (from Ref. [59]): the maximum for the ISGDR is at about 2 degrees, corresponding to 20 degrees in the laboratory frame; even though

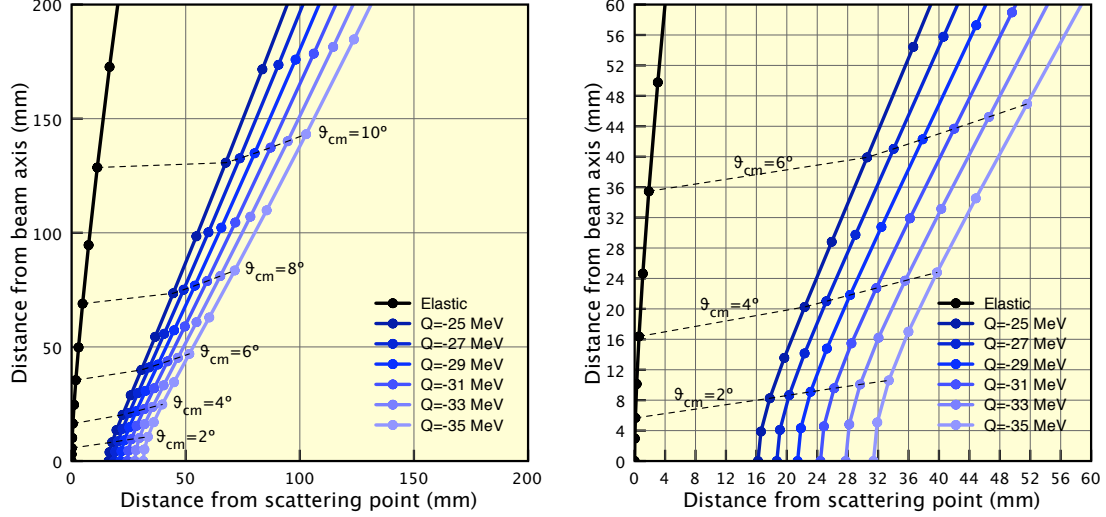


Figure 9: Loci of α particles scattered (at the origin point of the plots) by ^{56}Ni at 50 MeV/nucleon, both elastically and inelastically ($Q = -25$ to -35 MeV), after energy loss in a He-CF₄(5%) gas at 1 bar pressure. The energy loss calculations have been performed using SRIM [55]. In the blow-up on the right panel, the grid reproduces the maximum expected pad size for ACTAR.

those α particles have a low energy, about 1.5 MeV, they are well separated from the beam track.

An estimate of the statistics can be made using an average cross section of 10 mb/sr and assuming to detect particles between 2 and 10 degrees in the centre of mass frame. With a beam of 10^6 pps and a target thickness of 1.2×10^{21} at/cm² (50 cm at 1 bar) one comes to a yield of about one event per second.

Some remarks should be made concerning the efficiency of the detector. Once again, the heavy beam particles and the light recoils have different specific energy losses (see appendix A), however the problem is less severe than in other cases: ^{56}Ni at 50 MeV/nucleon deposits less 500 keV/mm, while the slow α particles of interest (10 MeV at maximum) deposit a few tens of keV/mm. This factor can be managed by the GET electronics. The same electronics would be capable of dealing with an incoming beam of 10^6 pps: the system would make a rapid pattern analysis of each event, and issue a trigger only for those events for which a signal was recorded outside the beam track. An actual limitation comes instead from the drift time of the primary electrons generated in the gas; usually drift velocities are in the order of a few cm/ μs , which sums up to a few μs to traverse an important volume such as that of ACTAR. After a scattering event, the following beam particle may enter the detector *before* all the electrons are collected, for example if an α particle was diffused in the direction

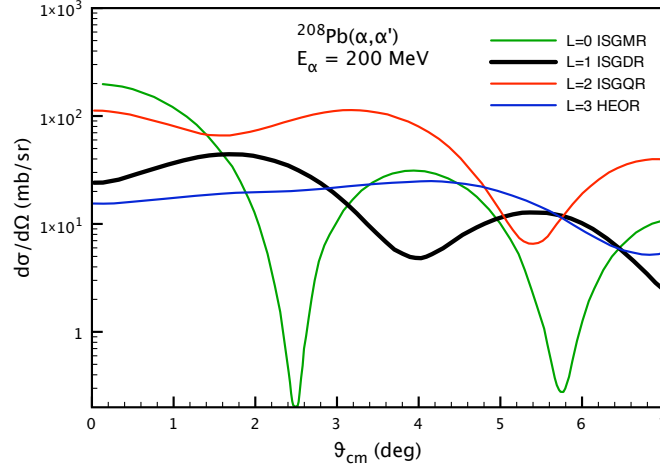


Figure 10: Differential cross sections for exciting isoscalar giant resonances via the (α, α') reaction on ^{208}Pb calculated using the distorted-wave Born approximation (from Ref. [59]).

opposite to the pad plane. The correlation between the beam particle and the light recoil is thus lost, and this can certainly be an issue for some measurements. In this case however, all the information is collected from the light recoil, and there is no need for a correlation: a beam rate of 10^6 pps can therefore be accepted. The final remark is about the detection of those α particles that, in the normal ACTAR configuration, are diffused “above” and “below” the beam with respect to the field direction: the much stronger beam signal would shadow theirs, and those events would be lost. The size of the beam shadow depends upon the spread of the beam signal on the pad plane: by using planar amplification systems (section 5.4) such a spread is completely negligible for what concerns the amplified signal (contrary to the induction from wires); and for the other possibility, that of a lateral *diffusion* of the electrons in the drift volume, both theory and simulations agree in estimating this to be a small effect, smaller than the pad size. The efficiency loss due to the beam shadow is then rather small, limited to a double “cone” occupying about 15%-20% of the full solid angle.

However a different arrangement of the drift field could be employed, orienting the field parallel to the beam. The beam projection on the pad plane would then reduce to a point, and all the recoil α particles (beyond, say, one degree in the centre of mass frame) would be visible. Such an arrangement, completed by a confining magnetic field, is the one designed for the TPC at MSU. In ACTAR, this would happen without the magnetic field. The arrangement is also presented in section 5.5.

As mentioned at the beginning of this section, a further interesting possibility in this kind of measurements is to observe the decay channels of the ISGDR and collect

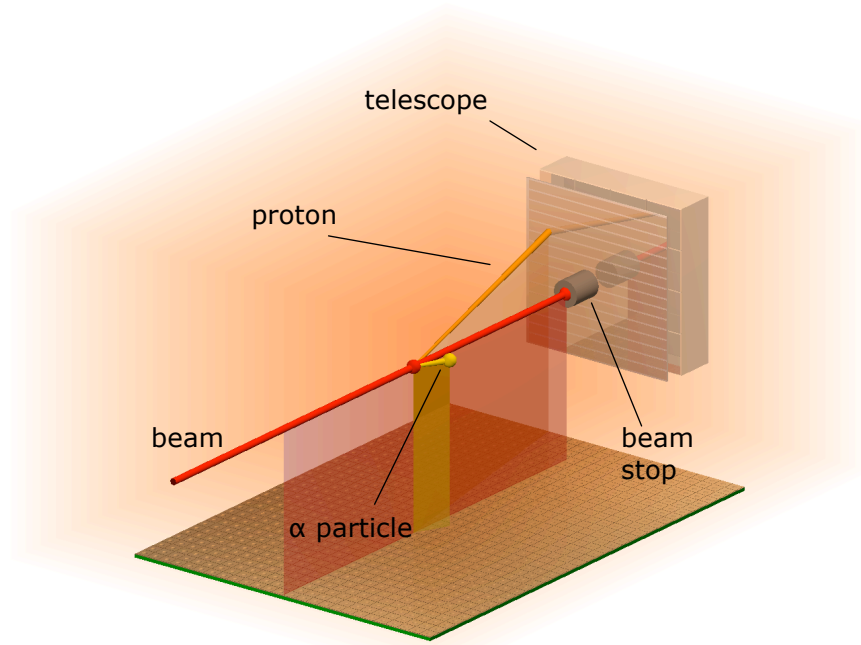


Figure 11: Configuration of ACTAR for the measurement of inelastic scattering on α particles and detection of charged particles emitted in the in-flight decay of the IS-GDR. The beam can be either stopped before the telescope (as shown), or leave the gas detector through a central hole in the telescope.

information about its fine structure; in particular we consider here the proton channels. With about 20 MeV available for the decay, protons are emitted in flight within a cone of almost 40 degrees aperture and with energies up to 130 MeV in the laboratory frame. Their energy loss varies between 1 keV/mm for the slowest ones (8-10 MeV) down to 200 eV/mm for the most energetic ones. Their detection in the gas together with the other particles is at the limit of the capabilities of ACTAR; in any case, protons are not stopped in the gas and only the use of ancillary charged-particle detectors can provide the energy information, which is necessary together with the angle to reconstruct the Q -value of the decay. For the protons which cannot be seen in ACTAR, a segmented Si-CsI telescope would be placed in the forward direction; the angular information could be reconstructed using the position on the Si detector and the position of the vertex of the inelastic scattering (a “delayed” correlation with the recoil α -particle can be restored using the proton signals as trigger). The efficiency of such a setup would depend upon the size of the telescope: a MUST2 module could reach about 20% efficiency. Such an arrangement is shown in Fig. 11.

4.4 Two-proton decay measurements

The decays of ^{45}Fe [26] and ^{54}Zn have been studied at GANIL/LISE3 with the Bordeaux TPC [24]. These measurements allowed to observe for the first time directly the two protons emitted. In addition, the energy sharing between the two protons and their relative angle are observables that are extracted from the data. Although the full analysis is not yet finished, it is clear that other nuclei cannot be studied at GANIL, simply because the production rates for other candidates like ^{59}Ge , ^{63}Se , and ^{67}Kr are too small in order to perform experiments on these nuclei.

However, in the future experiments with these nuclei can be performed at the BigRIPS separator at RIKEN. A proposal to search for these nuclei, to study their decay and to determine whether they are two-proton emitters is accepted at RIKEN and waits scheduling. In this first experiment, a silicon detector array will be used because of its simplicity and in particular because it allows to determine the total decay energy with high precision (typically with an uncertainty of 20 keV), whereas gas detectors only reach uncertainties of the order of 150 keV. Once one of these nuclei is discovered to be a two-proton emitter, it will be studied by means of a time-projection chamber in order to determine the individual proton energies and the proton-proton angle.

For this purpose, a TPC of length of about 50 cm is needed to stop all fragmentation products of interest in the active volume of the chamber. Due to proton ranges of only a few centimeters (2.5 cm in a gas mixture of 90% argon and 10% methane at atmospheric pressure), the chamber has to have a width and a height of about 10-15 cm only. However, the pad size should not exceed 2 mm to cover a sufficiently large number of pads for the low-energy protons in order to correctly define the traces of the protons. In the same sense, the projection time resolution has to be of the order of a few tens of nanoseconds to achieve the same resolution in the third dimension. In addition, due to the expected short half-life, the chamber, the electronics and the data acquisition should allow to treat two subsequent events within a millisecond.

As the two-proton emitters are produced in very tiny amounts (typically 1-10 per day), basically 100% detection efficiency is needed. This can be achieved due to the fact that unambiguous identification of the implanted nuclei is feasible by means of time-of-flight and energy-loss measurements. Then, these identified nuclei are correlated with their subsequent decays. This time and position correlation eliminates basically all background.

Although the different fragment separators used for this physics have very good performances in terms of rejecting contaminant fragments, the count rates at the end of these separators are nevertheless of the order of a few tens to hundred events per second. Therefore, the whole TPC system should be able to handle these rates.

A critical problem of the use of the ACTAR-TPC with two-proton radioactivity studies is the dynamical range needed to observe protons and heavy ions with the same setting of the gas and the electronics. A typical example is as follows: The heavy ion

(e.g. ^{59}Ge) at the end of its track has an energy loss of 10 MeV per 2 mm (the pad size). The following protons (typically 1 MeV) have an energy loss of 40 keV per 2 mm. Therefore, a dynamical range of 1000 is necessary if we do not want to saturate the electronics for heavy ion implantations.

With such an implementation of the ACTAR-TPC, a total number of two-proton events of some tens to hundred can be expected for a typical one-week experiment. As shown by past experiments [26, 60], this will be enough statistics to compare the experimental data to theoretical models in order to deduce the prime observables.

5 Design of the detector

The physics cases discussed in section 4 are based on the ambitious goals set for the performances of the ACTAR detector. In order to reach such performances, each aspect of the detector plays an important role: the geometry of the drifting field, the detection gas, the amplification technology, the use of ancillary detectors, the front-end electronic system for the data acquisition. One important aspect concerns the *modularity* of the detector: its main components (field structure, amplification module, pad plane) can be changed separately to obtain the optimal configuration for each measurement.

The breakdown of the detector in its components (Product Breakdown Structure, PBS) is given in Fig. 12. In this section, each element is presented and discussed.

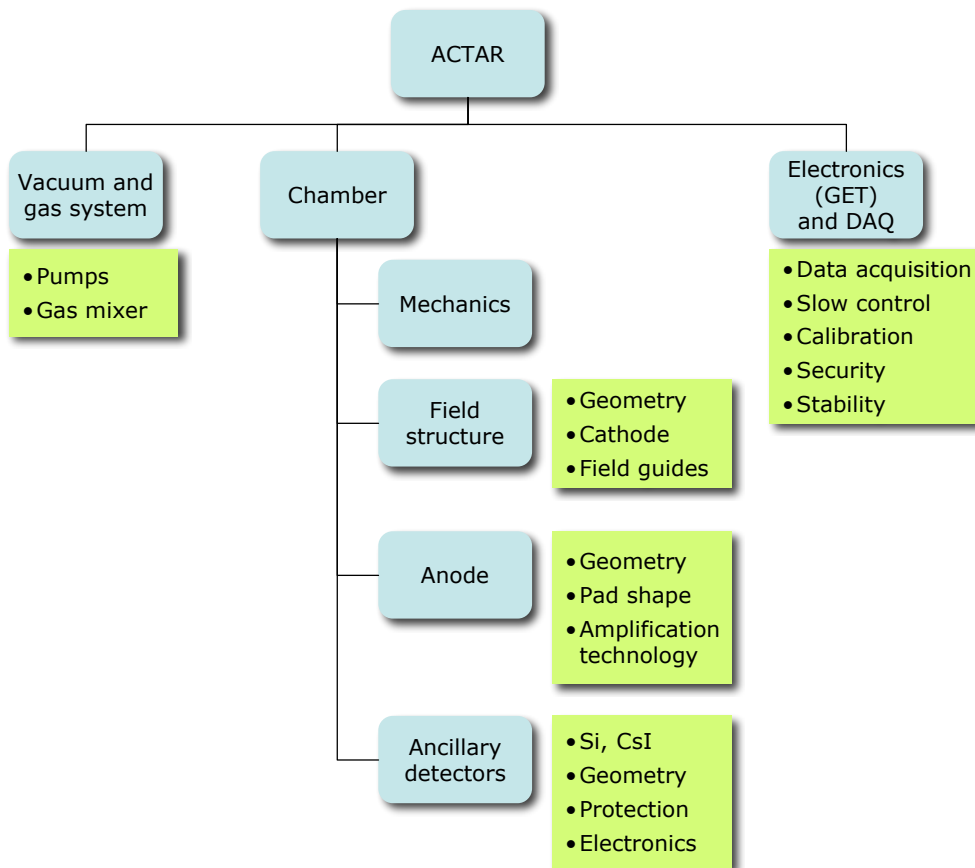


Figure 12: Product Breakdown Structure of the ACTAR detector.

5.1 Vacuum and gas system

The pumping station has to ensure the reliable operation and control of the gas flow in the detector. A continuous, adjustable flow is necessary, to avoid degradation of the conditions of the gas that may alter its detection properties. The pressure will have a double control, manual and an automatic adjustment to correct for temperature changes of the detection gas in order to keep a constant gas density. The unit will include a turbomolecular pump and a backing pump for the rapid evacuation of the detector chamber (volume about 150 l).

The gas control system will allow using pure gases and gas mixtures. The pure gases are typically isobutane (C_4H_{10}), hydrogen (H_2) and deuterium (D_2), used in reaction experiments where usually protons and deuterons act as target nuclei. Gas mixtures are used when it is necessary to improve the detection characteristics of the gas of interest: in decay experiments, methane (10%) is used with argon (90%); to study reactions with He nuclei as targets, a quencher is added. As for pumps, such a gas control system is standard equipment available commercially.

Because of the potential hazard of some gases, the gas handling system and the local infrastructure will have to ensure safe operations.

5.2 Mechanics of the chamber

The chamber contains the actual detector. It will have to be designed taking into account the following aspects:

- It has to accommodate and hold in position the detection volume, defined by the structure creating the drift field (cathode and field guides) and the pad plane, the ancillary detectors and the related cabling in the possible different geometric configurations (see further in 5.3). Easy opening and access to each component should be ensured.
- Coupling with magnetic spectrometers: the possibility to shield against the fringe field has to be taken into account.
- The flanges will allow the passage of electric lines for the high-voltage (for the fields and the ancillary detectors) and the signals. In particular the one for the signals of the pads has to be designed carefully, taking into account the specifications of the GET electronics. Another flange will allow the flow of the gas (entrance and exit).
- For calibration purposes, a laser will be installed with the possibility of inducing signals on all the pads. In addition, a system will allow introducing a calibration source into the detection volume without opening the chamber. An example of the latter system has already been designed for the MAYA detector.

- A temperature probe inside the gas volume will transmit its data to the pumping station for automatic correction of the pressure.
- At the interface with the volume of the beam line an entrance window will be present; the detection volume will have to be shielded from particles scattered on the window.
- The whole chamber should be certified for safe operation with pressures up to 3 bar and with explosive gases.

5.3 Field structure

The structure generating the drift field includes the cathode plate and the field guides (the amplification element and the pad plane are discussed further). The voltage applied (over a total field distance of about 30 cm) is typically 10-15 kV.

In order to allow the use of ancillary detectors for (light) charged particles escaping the gas volume, the structure holding the field guides should be as “transparent” as possible. The favourite solution is the use of thin Mylar foils (about $1.5 \mu\text{m}$ thick) with aluminium evaporated on the foil surface to form the conductive tracks. The technique is routinely used, for example for the large gas detectors built for the spectrometers at GANIL.

Different structures will be manufactured, having different field geometries, namely with the field lines either perpendicular or parallel to the direction of the incoming beam, to be used in different experiments. The design will be supported by simulations with appropriate codes such as Garfield [61] and Magboltz [62].

5.4 Amplification technology

As discussed in section 2.3, in order to ensure good performances (energy resolution and uniform response) and use different gas mixtures, a planar solution is the one of choice for ACTAR. With these methods, electrons are amplified in a high field zone that is oriented as the drift field. The electrons are eventually collected on the pad plane, which we will indicate from here on as *anode*.

Two solutions are attractive for ACTAR:

- *Micromegas* Micromegas (Micro-mesh gaseous structure) is a technology developed at Saclay [31]. The arrangement is illustrated in Fig. 13. A metallic micromesh, typically $5 \mu\text{m}$ thick, separates the drift space from the amplification gap, which is only about $100 \mu\text{m}$. The uniformity of the gap is obtained using different technologies [64, 65]; in the most recent versions, the spacers are pillars with diameters as small as $50 \mu\text{m}$.

A high electric field in the gap ensures the electron multiplication as shown in the

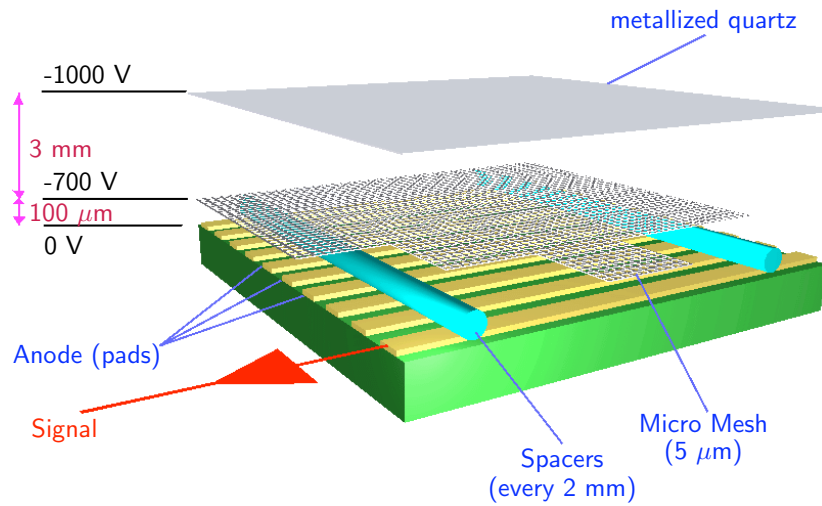


Figure 13: Arrangement of a Micromegas electron amplification device.

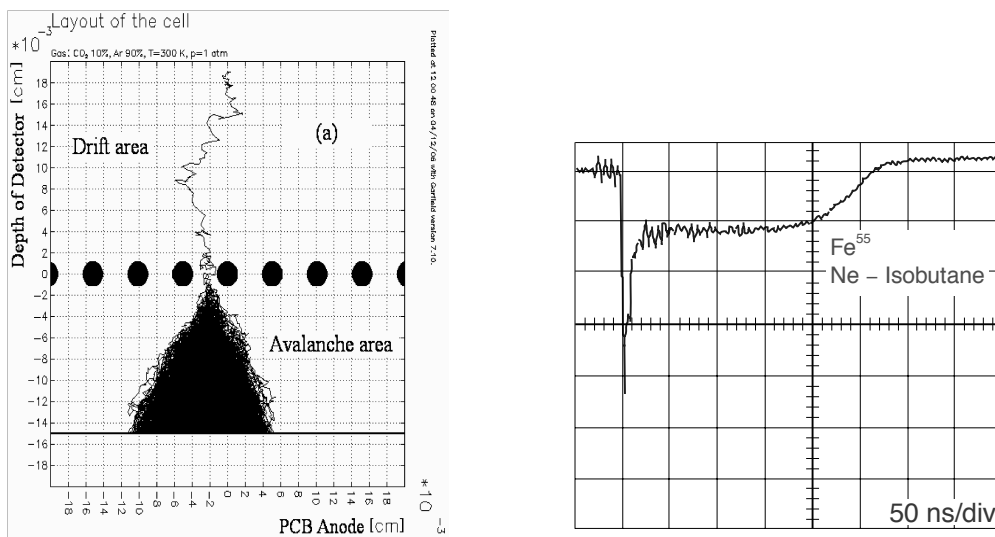


Figure 14: Left: simulation of the avalanche of an electron as it comes to the region of high field. Right: corresponding current pulse with the fast electron signal and the slower ion signal (taken from Ref. [63]).

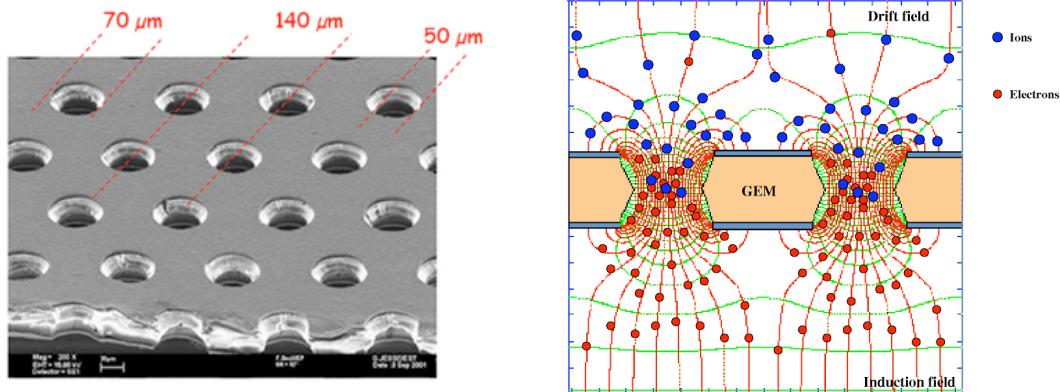


Figure 15: Left: electron microscope picture of a GEM device. Right: sketch of the working principle of a GEM.

simulation on the left panel of Fig. 14. The signal recorded on the anode, on the right panel of the same figure, has a very fast component (less than 1 ns) due to the collection of the electrons, followed by the induction due to the movement of the ions; the latter is however also reasonably short (about 200 ns) because of the reduced size of the gap (ions are almost entirely collected on the grid). Besides the high rate capability, these detectors have proven very robust, as discharge is not destructive [66]. Gains reach easily factors from 10^3 to 10^5 , with an intrinsic resolution that in some conditions can be better than 1% [32]. Another not negligible advantage is that the manufacturing is rather inexpensive: the cost is of the order of 5 €/cm².

- *Gas Electron Multipliers (GEMs)* GEMs were designed at CERN [25]. An electron microscope picture of such a device is shown in Fig. 15: it consists of a Kapton foil, 50 μm thick, covered with copper on each side, and perforated by bi-conical channels. A voltage (some hundreds volts) is applied between the two surfaces; the field lines focus through the hole, where the field intensity reaches values which are sufficient to trigger the electron multiplication. The electrons are then driven by a transfer field to the anode (on the bottom in the picture), giving a very fast signal with almost no tail due to the positive ions. The GEM holes are totally free after less than 1 μs, allowing detection at high rates. An advantage of the GEM configuration is the flexibility, as they are de-coupled from the anode. For example, even though it is possible to obtain large gains employing only one GEM, usually two or three GEMs are arranged in cascade and operated at lower voltage, with a significant improvement in stability. As for Micromegas, GEMs too are relatively inexpensive (less than 1000 € to equip an area like the anode of ACTAR).

The two devices, collectively called micro-pattern gas detectors, have similar performances; the differences may depend on the operating conditions (type of the gas, voltage applied). Micromegas has shown higher breakdown limits [67]. Since these detectors were conceived mainly for the measurement of high-energetic leptons, not much is known about the performances in presence of much stronger signals such as those induced by light and heavy ions. For example, for ACTAR we are interested in the energy resolution for such signals. For this reason, tests with the two modules are foreseen in the course of the ACTAR project (section 6.1.3).

The tests investigate the performances (gain as function of applied voltage, discharge limits) for different gas mixtures, in search of the optimal conditions for the detection of the signals of interest in the various physics cases identified for ACTAR. The first measurements have already been carried out at IPN Orsay with a Micromegas module on a pad plane, and with various gas mixtures containing He; the results are part of the report of the ACTAR JRA [5]. Other tests have started at GANIL.

One feature of particular interest concerns the possibility of having different gain factors in well-defined areas of the amplification zone. Typically, this would allow the simultaneous detection of the very strong signals from a heavy beam particle along the projection of the beam trajectory, and of the much weaker signals from the scattered light ions. This may be achieved for example with GEMs, placing (additional) modules outside the region of the beam projection. With Micromegas, there is the possibility of using the coupling to the anode by applying different bias voltages on the pads in the different regions, thus effectively modifying the value of the amplification field; another method consists in using a special micro-mesh, formed by weaving together metallic wires in one direction and insulating ones in the other, to give the possibility of applying a different voltage in separate areas.

5.5 Anode

The anode collects the electrons generated in the amplification zone. It is segmented into pads, in order to allow the independent collection of energy and time information from more than two tracks.

By using GEMs or Micromegas, the amplification zone is very close to the anode surface. Because of this and the field orientation, there is no spreading of the electron signals on different pads as it happens, for example, using wire amplification in MAYA. This means that the size of the pads represents the limit to the spatial resolution. More precisely, for a given particle energy the resolution depends on the ratio between the size of the pads and the length of the tracks in the gas, where the latter is determined by the gas pressure. In principle, and within certain limits, these quantities can be scaled together with the size of the whole anode, resulting in about the same performances. It has already been discussed in section 2.3 that mechanical constraints limit the minimum size of the pads, to accommodate the connectors; on the other hand, the area that is

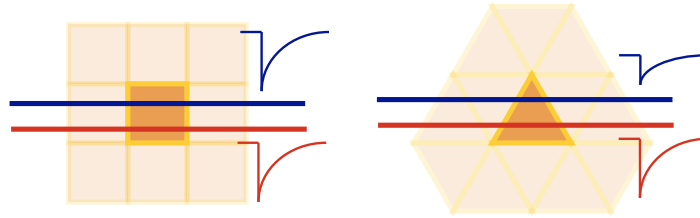


Figure 16: Effect of the pad shape: on the square pads (right) the two tracks induce the same signal. By using a triangular form (right), the two signals differ, because the fraction of the projection on the pad depends on the position. The information can be correlated with that of neighbouring pads to increase the resolution.

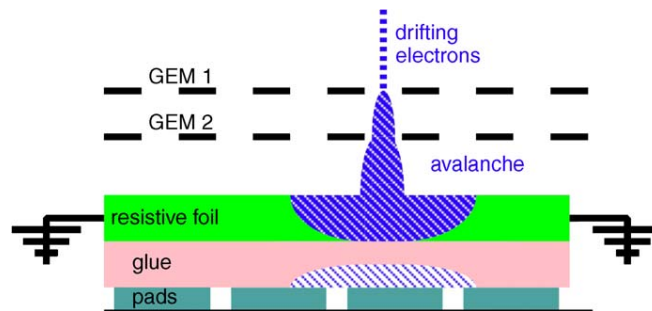


Figure 17: Scheme of a double GEM amplifier and anode with resistive layer (from [68]). The charge is distributed on the neighbouring pads.

covered by ancillary detectors should not be too large.

The present technology certainly ensures a pad size of $4 \times 4 \text{ mm}^2$, and other solutions are being considered that would allow a smaller size. In parallel, other methods are at study to improve the spatial resolution beyond the limit imposed by the size. Two ways are being considered:

- An adapted design of the pad shape: the principle is illustrated in Fig. 16. For certain pad shapes, it is possible to extract more precise information about the position of the track on the pad. In practice, this method requires a very good calibration and uniform response of the pads. The influence of the electronic chain can be important; such effects will be investigated.
- Use of a resistive layer on the pad plane: the resistive layer has the effect of spreading the charge on a larger area, to the neighbouring pads (see Fig. 17). The centre-of-gravity method can then be applied to derive the centre of the distribution, with a precision better than the pad size. This technology is being developed

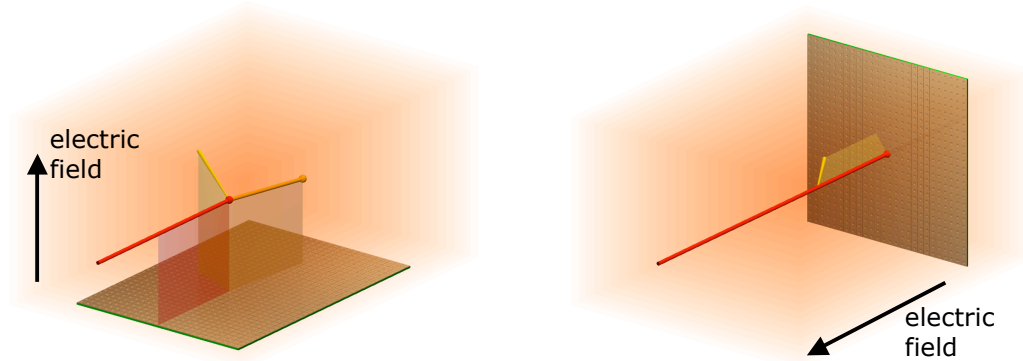


Figure 18: Left: planar configuration, with the field perpendicular to the beam direction. Right: axial configuration.

by several groups (for example see Ref. [68]) with very encouraging results: it was possible to achieve resolutions of $1/40$ of the pad size. The disadvantages are a worse separation of tracks; and, especially, a change of the time characteristics of the signals, with a rise time that is in the range of a few hundreds nanosecond.

The cost of anodes, like for amplification stages, is affordable. This will allow investigating the solutions mentioned above with tests employing several different anodes, besides using simulations. In fact the intention is to produce different anodes, satisfying the needs of the various physics cases. As we have seen, this flexibility will be a characteristic of the whole detector. An example is shown in Fig. 18, where two geometries are shown, with the field perpendicular to the beam direction (planar configuration) or parallel (axial configuration). The second arrangement is useful to minimize the projection of the beam tracks.

5.6 Ancillary detectors

Charged-particle detectors can be placed around the drift volume to catch the escaping ions. The tracks of such particles would still be visible in ACTAR, providing the position information; the ancillary detectors would complete the information about the energy of the particle. Identification of the particle could also be made, using the recorded $\Delta E-E$.

The ancillary detectors should have an energy resolution at least comparable with that of ACTAR, while a high segmentation is not required. For backward angles, where only low-energy light particles are expected, silicon detector are the obvious choice. For intermediate and forward angles, multiple-stage detector would be necessary to stop the most energetic light particles. As with other components, the configuration of

these detectors will be adaptable for different measurements, covering the angles where the particles of interest are expected. Thus it will not be necessary to reach a complete coverage of the whole detector.

Even though there is no need for a high segmentation, the area of each silicon detector should not be too large, to avoid a large capacitance and preserve a good energy resolution. Even with detector sizes of the order of a few centimeters on each side, the total number of channels would easily run into the hundreds. A very interesting option for the electronics of the ancillary detectors is that developed for MUST2 and also used in MUSETT, based on ASIC chips. It is an integrated solution, with all the electronics concentrated on a card which manages a large number of channels in a multiplexed mode. This would provide a reliable system, greatly reducing the amount of cabling inside and outside the detector. An attractive possibility would even be that of integrating the ASIC chip of MUSETT (ATHED) into the GET electronics.

An issue to be considered is that of insulation of the surface of the ancillary detectors from the drift field. We already mention in section 5.3 that, to ensure transparency for the escaping particles, the field guides would be metallic strips evaporated on thin Mylar foils. A second, insulating Mylar foil can be accommodated between the first and the surface of the detectors, increasing protection and reducing the chance of discharge.

Size of the ACTAR detector

Clearly the cost of the ancillary detectors is a crucial factor in the determination of the overall size of ACTAR. From the point of view of performances, the physics cases illustrated in section 4 show that such results can be achieved when a spatial resolution of 2 mm is attained in a detection volume which is roughly a 30 cm-size cube. Such spatial resolution should be feasible with pads with a linear size larger than 2 mm – possibly already with $4 \times 4 \text{ mm}^2$ pads.

Still, it is obviously important to explore all the possibilities to reduce the overall dimensions of ACTAR by reducing the pad size further. If the technology allows $2 \times 2 \text{ mm}^2$ pads, the size of the detection volume could be safely reduced to a box of about $20 \times 20 \times 20 \text{ cm}^3$. The number of ancillary detectors that the collaboration intends to acquire, combined with the existing ones already available from the partners (see section 6.3) would allow a coverage of such a volume at the level of 40%, thus already very interesting to perform the measurements discussed as physics cases for ACTAR.

5.7 Detection gases

The choice of the main component of the detection gas is dictated by the requirement of the physics case. For reaction measurements, the gas should be mainly composed of atoms of the target nuclei; for decay studies this constraint is not present, and an element with a high stopping power is chosen. The list of gases, as function of their use, includes a) isobutane (C_4H_{10}) or pure hydrogen (H_2) for reactions on protons, b)

deuterium (D_2) for reactions on deuterons, c) helium (He) for reactions on α particles and ^3He , and d) argon (Ar) for decay studies.

A good detection gas should fulfill several requirements: operation at a low voltage, high gain, good proportionality, rapid drift time for electrons, high rate capability. To reach optimum performance, we have the following possibilities:

- Change the gas pressure: all other parameters the same, lower pressures correspond to higher drift velocities. The effect on the gain, on the other hand, is not trivial. For example for Micromegas, one can show that there is an optimum value of the pressure [69]: below it (which translates in lower density of the gas atoms) the number of electron multiplications becomes small in the amplification gap; above it, the electron mean free path is short and electrons do not reach enough energy to trigger a multiplication.

As a general rule however, the pressure should be chosen to optimize the physics goals: to have a high target thickness but preserving a good spatial resolution; a density sufficient to stop the incoming beam or outgoing particles as necessary.

- Change the drift field: within some limits (a few hundreds kV/cm, depending on the gas), the drift velocity of electrons scales with the ratio E/p , where E is the drift field and p is the pressure. Given the size of ACTAR, we expect to work in such range; therefore the pressure and the drift field can be scaled together keeping the drift velocity constant.
- Change the amplification voltage: in most cases the gain factor increases exponentially with the applied voltage. To detect the weakest signals, one would normally choose the highest possible voltage, just below the discharge limit. However, with the signals generated by heavy ions, the gain may be even too high for the electronics of the pads. The correct gain needs be found for each case. In this respect, it is important to build a database with this information.
- Change the composition of the gas: even small quantities of a second gas can change the properties of the mixture dramatically. For example, tetrafluoromethane (CF_4) can be added to He to decrease the average energy necessary to create an electron-ion pair, and thus obtain a better energy resolution; the drift velocity also increases significantly, and effects are present on the gain factors. For the same reasons, methane (CH_4) is normally used in mixtures with argon. If ACTAR is used as an active target, the added component should be kept as small as possible, to reduce background reactions.

The test measurements foreseen within the ACTAR project (section 6.1.3) aim at the determination of the best conditions with respect to these parameters, in particular with attention to gas mixtures.

5.8 Electronics and data acquisition: the GET project

The electronic system for the collection of the pad signals is of key importance for ACTAR. The reasons were discussed in section 2.3; Table 1 summarizes the parameters on which the electronics can play a role. Already within the work of the ACTAR JRA it became clear that a system having all the desired features would have to be a newly developed one. For this reason a dedicated project was started: GET, General Electronics for TPCs [6]. A proposal submitted to the French National Research Agency (ANR) has been accepted recently. This ensures that a prototype of the system will be designed, built and tested in the next four years.

We recall here the main features of GET, its performances and the architecture.

GET is designed from the start to be a very flexible system. It takes into account the needs of different detector devices, planned or under construction for measurements at low and medium energies (ACTAR, the AT-TPC at MSU) and high energies (at FAIR and RIKEN). The main characteristics are:

- A very high density at the front-end, where up to 30000 signals can be collected from a small volume. Beyond the needs of ACTAR, the system is foreseen for use with future, larger detectors also in high-energy physics.
- An unprecedented dynamic range, to cope with the very different signals generated in the gas: the ratio between the energy deposited by heavy incident beam particles and light recoil nuclei can be as much as 3 orders of magnitude.
- An internal trigger possibility. In some experiments all the particles will be stopped in the gas volume requiring this feature, not available in present TPCs.
- The possibility of recording the whole signal shape: the time evolution of the signals can provide additional information regarding the spatial properties of the track (for example to identify long tracks almost perpendicular to the pad plane). The system will *sample* continuously the signals from the pads; to cope with the different conditions of operation (different gases, pressures and drift fields, that determine a large range of drift velocities), the sample rate can be adjusted between 1 MHz and 100 MHz.
- A high data rate: the goal is to reach 1 kHz of accepted events. The corresponding data throughput is very large (of the order of almost 1 Gbit/s) and has to be handled by very fast connections (optical links are being used) between all the parts of the system, but also by an effective data reduction at the beginning of the electronic chain. This implies that each event needs to be pre-processed to select only the events of interest, by employing fast algorithms implemented on the front-end cards.

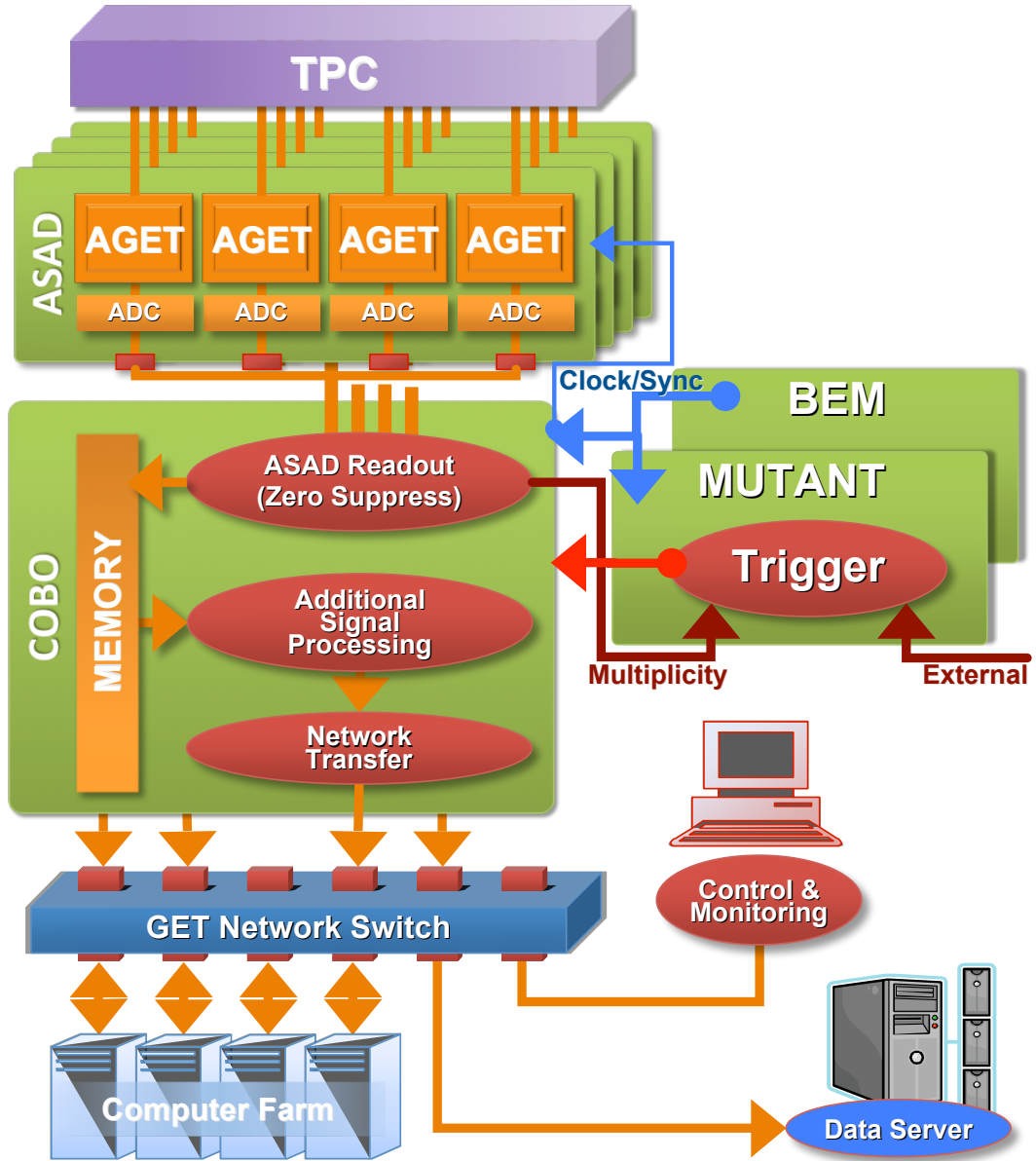


Figure 19: Schematic view of the GET system and its different parts. The ASAD and COBO modules read out and process the data, sending them over a network after validation by a multiplicity processing system.

In many respects, these features make of GET a unique system in nuclear physics.

The architecture of the system is shown in Fig. 19. At the core of the system there are ASIC chips named AGET, that process continuously the signals from the pads (sampling at adjustable rates) through a preamplifier (which can be bypassed) and shaper (with adjustable gains), and keep the information in a circular buffer (512 cells or less, programmable). A special feature foreseen for decay measurements is that of splitting the buffer in two parts, the first to record the implantation event and the second for the decay (within a programmable time), without performing a read out in between and hence reducing the dead time to a very minimum. The buffer is read out upon a trigger, that is originated from the signals provided by a discriminator in AGET. Each AGET handles 64 channels. The front-end card ASAD accommodates 4 AGET and their corresponding ADCs (12 or 14 bits). The low-level trigger from the pads is passed to the multiplicity and trigger card (MUTANT) that performs a fast (programmable) pattern analysis and selects the events of interest. For a selected event, the concentration cards (COBO: one card for 4 ASAD) perform the readout of the data, a compression, and then send the information through a fast switch to a computer farm for further processing and storing.

The MUTANT card can also trigger the system upon external signals, for example those provided by beam detectors or ancillary detectors. The back-end card BEM has the function of providing a clock that can be internal or external, acting possibly as an interface to other data acquisition systems for their synchronization.

The system can be scaled: up to 9 COBO cards can be driven by a single MUTANT (thus 9216 channels), and the system can be expanded up to three MUTANT cards.

Included in GET there is a control and monitoring system, through which the parameters of AGET (gain, threshold, sampling rate, buffer size, configuration for decay measurements), COBO (data processing and compression) and MUTANT (trigger algorithm) can be controlled. A way to automatically adjust the parameters of AGET depending on the signal pattern (as elaborated by MUTANT) is under investigation.

The GET project will produce a prototype, to be tested with a TPC in an actual physics experiment in 2012. The ACTAR project includes such test in its timeline.

At the interface between GET (the ASAD card) and ACTAR (the anode), the physical connection has to be studied to handle the high density of the pads. Such connection has to include a device to protect the electronics from discharges occurring in the gas; this is not included in the GET baseline project, because it may depend on the detector (GET may be used for other types of detectors, like solid state ones). The arrangement of the connectors is also important: depending on the expected occupancy of the pads for a typical event, the occupancy of each COBO should be minimized to increase the rate of the data flow. These aspects will be tested within the ACTAR project.

6 Planning

This part presents a first plan for the ACTAR project. The timeline (section 6.2) is consistent with that of the GET project, and takes into account the milestone of the SPIRAL2 Preparatory Phase for the signature of a Memorandum of Understanding (MoU). Concerning the resources (costs and manpower), a first evaluation is presented; more accurate figures, including a breakdown into the participation of the different partners, will be made after the consolidation of the collaboration and in view of the signature of the MoU (Sep 2010).

6.1 Organisation - WBS

The Work Breakdown Structure (WBS) of the ACTAR project is shown in Fig. 20. Table 2 gives the deliverables for each work package (WP). Here, like further when discussing the resources, we do not indicate the assignment of activities to the partners of the collaboration, because this aspect is still under discussion.

We present now the tasks and goals within each WP.

6.1.1 WP1 - Coordination

The coordination group will be typically composed of four people. Its duties are:

- Control the advancement of the project, coordinate the tasks;
- Keep a record and manage the available resources (finances and manpower).
- Inform the collaboration of the status of the project, through regular reports and organizing periodic meetings. One general collaboration meeting will be held in the fall of each year.
- Manage the relations with external parties such as future users;
- Promote and direct the negotiations to reach the signature of a Memorandum of Understanding (MoU) between the partners. The MoU will include the guidelines for the management of ACTAR and its routine use after the completion of the construction and commissioning phase.

6.1.2 WP2 - Physics support

The main aim of this WP2 is to define the physics specifications of ACTAR, and ensure that they are implemented in the design. This work follows and builds upon the output of the ACTAR JRA, where the range of interest for the new active targets was identified along with specific physics cases. This WP will develop in further detail those cases, arriving at the final list of the performances required from the detector.

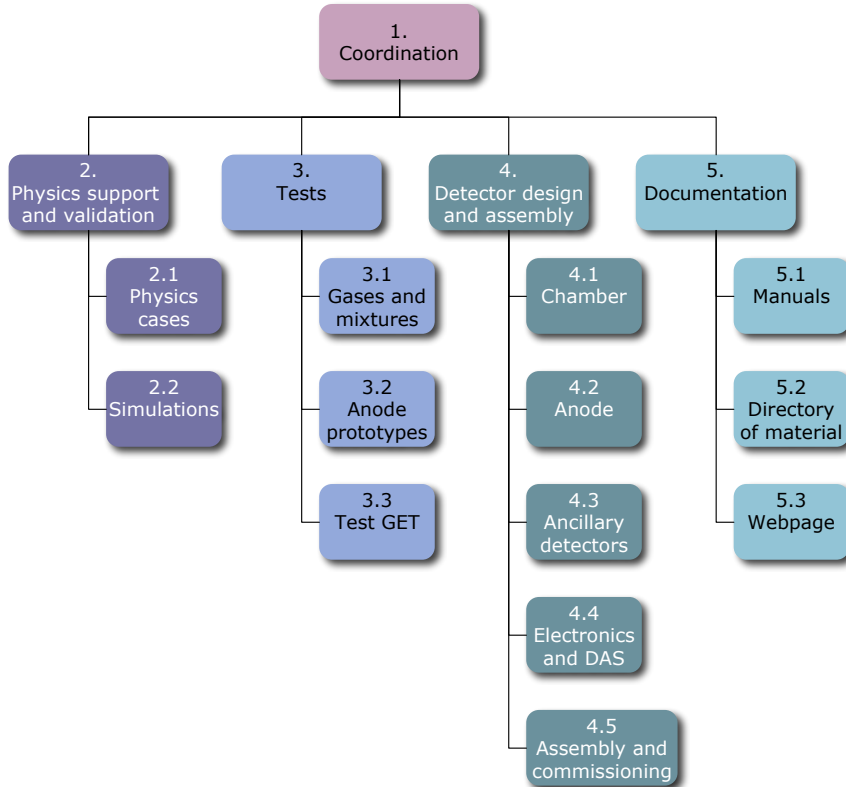


Figure 20: Work Breakdown Structure for the ACTAR project.

Table 2: List of the deliverables for each work package.

WP	Deliverables	Date
WP1	- Periodic status reports - Memorandum of Understanding	Every 6 months Sep 2010
WP2	- Report: physics cases	Dec 2010
WP3	- Report tests gas mixtures - Report anode prototypes - Report test GET	Dec 2010 Dec 2010 Dec 2012
WP4	- Technical design: chamber - Technical design: anode - Technical design: ancillary detectors	Jun 2011 Jun 2011 Jun 2011
WP5	- Complete documentation	All phases

The WP2 will coordinate the work of two auxiliary tasks.

- *Task 2.1 - Physics cases* The list of the physics cases will be evaluated in view of the experimental and theoretical development in the field. The preliminary selection (section 4) will be validated or changed in function of the relevance of the scientific results that each measurement can bring.
- *Task 2.2 - Simulations* Each physics case will be studied through a complete simulation of the related measurement as performed with ACTAR. The simulation will eventually determine the values of the parameters for the ACTAR detector, that will allow reaching the desired results in terms of accuracy, statistics, resolution. The package ActarSim [51], developed within the ACTAR JRA, will be used for this purpose.

This WP2 will provide the guidance for the other WPs in the project: besides producing the basis for the design of the ACTAR detector (WP4) it will also follow closely the activities of WP3 (tests). Possible technical constraints, either from the tests performed within this project or from the specifications of the GET electronics, will have to be taken into account in the evaluation of the detector possibilities. For this purpose, regular communications with the tasks in WP3 and with GET will be kept.

The deliverable of WP2 is a report containing a) the final characteristics of ACTAR (required performances); b) a list of key experiments with motivations and expected results.

The report will be made available for the start of the technical design of the detector. The activity of WP2 will still continue afterwards, keeping a supervision of the tests (prototype and GET). Eventually, this activity should evolve into a support forum to promote and guide the physics to be performed with ACTAR.

6.1.3 WP3 - Tests

A series of test measurements will be performed to investigate the possible solutions for some aspects of ACTAR, in particular concerning the *detection gases* (and gas mixtures, section 5.7), the *amplification technology* (section 5.4), and the design of the anode. In addition, an experiment is foreseen to test the full prototype of the GET electronics (section 5.8) in line with the schedule of the GET project.

The tests will make use of the existing MAYA active target and Mayaito TPC. Mayaito is a small chamber, about $30 \times 3 \times 3$ cm³, which was designed to measure the range of incoming ions in various gases.

Three tasks are identified within this WP:

- *Task 3.1 - Gases and mixtures* The properties of the gases and gas mixtures of interest will be investigated, to build a knowledge about their characteristics. The

aim is to find the best operating conditions for the possible experiments (target thickness, background reactions, drift velocity of the electrons, gain) by varying the pressure, the applied voltages, and the composition of the mixtures. The first tests of these kind already took place at IPN Orsay. At GANIL, both MAYA and Mayaito will be used (tests with Mayaito are already in progress at GANIL; measurements using MAYA are planned in the fall of this year).

A report will be produced at the end of these tests (end 2010).

- *Task 3.2 - Anode prototypes* For this task, various anode prototypes will be manufactured, together with the corresponding amplification modules. Concerning the latter, Micromegas, GEMs, and a combination of the two will be tested with the aim of controlling the gain in different regions of the pad plane. For the anode, the aspects illustrated in section 5.5 will be studied, namely the resolution limits for different pad sizes. This will offer the chance of verifying solutions which are at study to use smaller sizes than $4 \times 4 \text{ mm}^2$, in conjunction with the first prototypes of the GET front-end cards (ASAD), which will be available in 2010. These tests will provide an essential feedback to GET for possible modifications of ASAD or its components. It is noteworthy to mention that tests with the ASAD card will also be performed at MSU, in the framework of the development of the MSU AT-TPC [7]; both active target projects, and of course GET, will benefit from the strong exchange of information which is in place between the collaborations.

A report will be produced in correspondence with the ones from task 3.1 and WP2, to serve as basis for the design of the anode of the ACTAR detector (WP 4.2). After the report, further tests will be still carried out, in the framework of the GET project, of the new-version prototype cards of the system.

Mayaito, with its compact dimensions, is a convenient device to perform the tests for this task; a system is already in place that allows changing the anode and amplification stage, and the manufacturing of new modules is rather quick and inexpensive. The first anode equipped with Micromegas is already available. It is not excluded that a larger anode is built for tests using the MAYA assembly.

- *Task 3.3 - Test GET* This task is shared with the GET project. The aim is to test and validate the prototype of the GET electronics; the test is an actual physics case experiment to be performed at an accelerator facility. The detector will be composed of a version of the ACTAR anode, having the required high pad density. The MAYA chamber is the one of choice for installing this anode.

6.1.4 WP4 - Detector design and assembly

This WP is central, as it concern the actual manufacturing of the ACTAR detector. The subdivision into tasks essentially follows the PBS (section 5).

- *Task 4.1 - Chamber* The design of the chamber will respond to the criteria listed in section 5.2. The task includes the design of the structure holding the field cage (section 5.3), the mechanics for the ancillary detectors, and the calibration devices (source, laser). A complete technical design will be produced before the construction phase.
- *Task 4.2 - Anode* This task is responsible for the design and manufacturing of the anode or anodes, following the specifications provided by the reports of WP2 and WP3. This part includes the pad plane and the amplification technology, since the two elements are connected. A technical design will be produced.
- *Task 4.3 - Ancillary detectors* Aim of this task is to define, starting from the physics specification of ACTAR, the required system of ancillary detectors to be put in place around the gas volume (section 5.6). The study phase will be concluded by a technical design. The acquisition of the detector will take place in phases; the first measurements will also employ detectors made available within the collaboration.
- *Task 4.4 - Electronics and DAQ* The electronics of the system will be designed and tested within the GET project. This task will provide a GET system tailored to the ACTAR detector, purchasing the necessary electronic components and the computing facilities for the Data Acquisition and Control system (DAQ).
- *Task 4.5 - Assembly and commissioning* The assembly will proceed with the arrival of the components (electronics and ancillary detectors). An important commissioning task will have to be performed on the electronic components.

6.1.5 WP5 - Documentation

This WP deals with the aspects relative to the collection and distribution of information, both within the project and to external parties. It comprises three tasks.

- *Task 5.1 - Manuals* This task ensures the collection of all the information about the hardware and software of ACTAR. User manuals, technical designs and reports. It also carries the responsibility of verifying that the documentation is complete, and take the necessary steps to ensure this goal.
- *Task 5.2 - Directory of material* A list of all the material related to the ACTAR detector will be made and then constantly kept up to date. This task will continue after the end of the project (commissioning of the detector).
- *Task 5.3 - Webpage* The ACTAR webpage will have a public section, dedicated to the presentation of the detector to the public; and a private one, which will collect the documents mentioned above plus internal news concerning the project,

such as minutes of meetings, reports on the status of the project. The webpage will be maintained past the commissioning of the detector, as a communication instrument for the collaboration.

6.2 Timeline

The timeline for the construction of ACTAR is shown in Fig. 21. A summary of the expected timeline of the GET project is also given, as its development closely concerns the ACTAR project.

As mentioned in the introduction, the collaboration is in a phase of consolidation. In this process we benefit from the framework provided by the SPIRAL2 Preparatory Phase project, that offers support for organizing purposes.

Beginning in the second half of this year (2009) and for a period of two years, the collaboration will work on raising the funds necessary for the realization of this project. The partner laboratories and institutes will apply to their own financial Institutions, backed by the collaboration as a whole. During this period, negotiations will be carried out to reach the signature of a Memorandum of Understanding, that will define the terms of the commitment of the partners in the collaboration and will set up a structure to manage the future of the ACTAR detector once it will have become operative. These activities are coordinated within WP1.

The physics support (WP2) will be active throughout the duration of the project, and beyond to eventually become a permanent forum with propositional and advisory duties. It will interact with WP3 (guidance and feedback of tests) and WP4 (technical design of ACTAR), and will produce a report in December 2010 describing the performances of the detector and the expected physics results.

The tests (WP3) of the gas mixtures and the anode prototypes are articulated as illustrated in section 6.1.3 (the first tests with Mayaito are already in progress). The tests of the anode include those for the amplification technology and the first tests of the ASAD prototype (2010). After the reports in December 2010, tests of the GET prototype cards will still be possible. The final test of the whole GET system will be performed in 2012 using a version of the ACTAR anode.

The design of the parts of the ACTAR detector (WP4) will move from the reports produced in December 2010. The design of the chamber, however, will start earlier, for the definition of those mechanical aspects independent from its contents. All technical designs will be completed in June 2011. They will be followed by the construction phase; for the anode, a version to be used with an existing chamber (like MAYA) will be produced by the beginning of 2012 for the test of GET.

The assembly of the detector and commissioning of the GET components will take place in the second half of 2012 and first half of 2013.

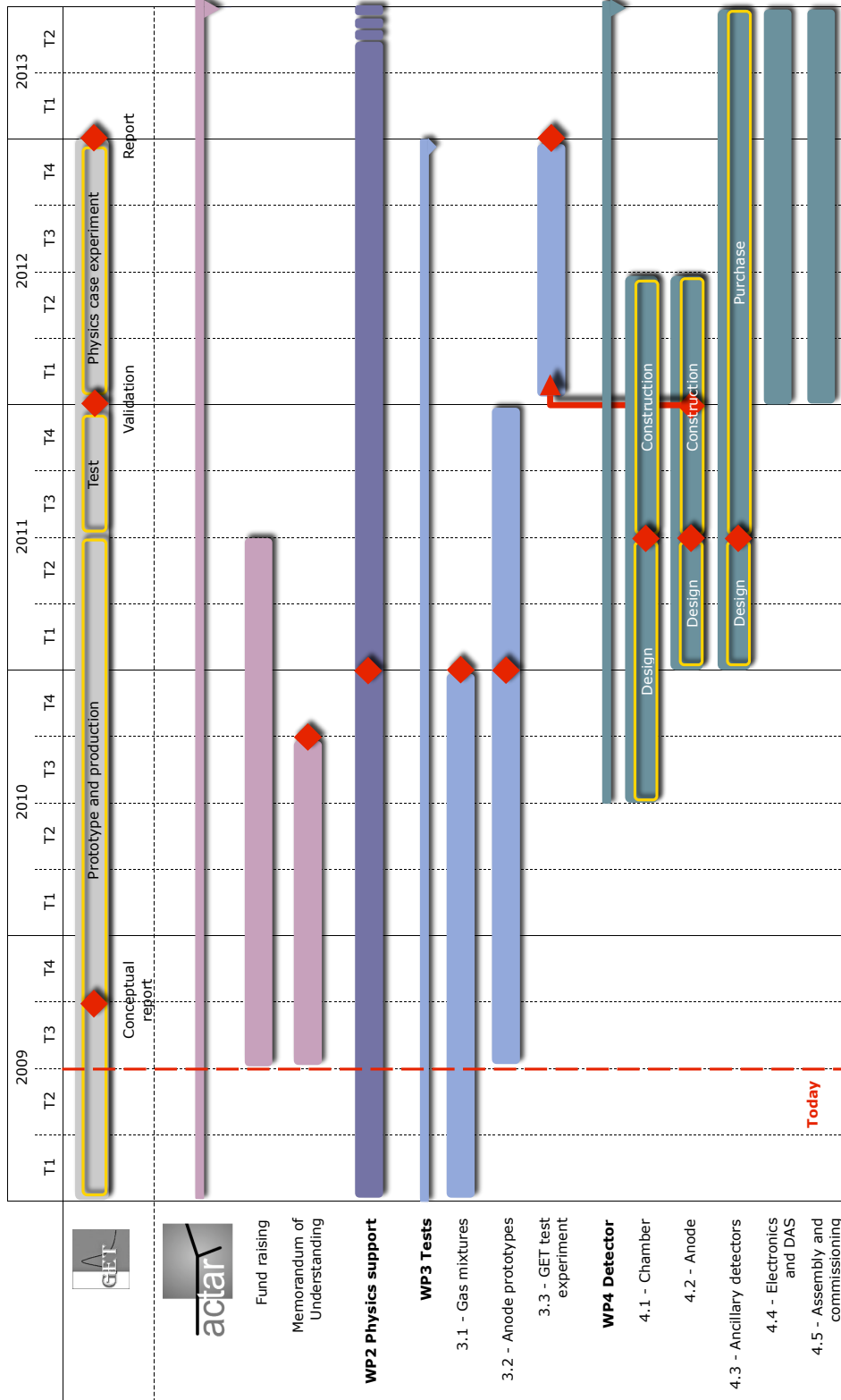


Figure 21: Timeline of the ACTAR project.

Table 3: Description of the costs for the project, in k€ (manpower not included).

WP	Description	Cost
WP1	Meetings, communication	20
WP2	Meetings, communication, visits	24
WP3	Anode protoypes	31
	non-GET electronics	35
	Total WP3	66
WP4	Gas handling system	20
	Calibration Laser	30
	Mechanics (incl. chamber)	40
	Anode	20
	Ancillary detectors (4× MUST2-type)	120
	non-GET electronics	50
	Computing	10
	GET electronics	300
	Total WP4	590
Total		700
Existing ancillary detectors:		
	Huelva (Si $\Delta E-E$)	150
	MUST2 (8× Si-CsI telescopes)	200
Total cost of the project		1050

Table 4: Detail of costs per year (k€).

WP	2009	2010	2011	2012	2013	Total
WP1	4	4	4	4	4	20
WP2	6	6	6	6	–	24
WP3.1	2	2	–	–	–	4
WP3.2	2	45	5	–	–	52
WP3.3	–	–	–	10	–	10
WP4.1	–	–	90	–	–	90
WP4.2	–	–	20	–	–	20
WP4.3	–	–	50	50	20	120
WP4.4	–	–	–	300	60	360
Total	8	59	167	372	84	700

6.3 Resources

Tables 3 and 4 present a summary of the estimated costs (excluding the cost of manpower), and a distribution along the duration of the project. The main expenses are those for the GET electronics and for the ancillary detectors. For the latter, we intend in a first phase to acquire four three-stage telescopes (DSSD+Si+Si; the cost includes the associated MUST2-type electronics), and to integrate them with existing detectors available from within the collaboration; in particular, detectors from Huelva (Spain) and from the MUST2 collaboration. The cost of these detectors is explicitly added in Table 3 to obtain the total cost of the project. In a further future, outside the time frame of this project, other telescopes will be added.

In Table 5 the summary of the required manpower is given; the detail for each task is presented in Table 6. Concerning the physicists involved, there are two tasks (WP2.2 Simulations and WP3 Tests) where a large time occupation (50%) is required. These positions could typically be fulfilled by postdocs hired for the specific task.

The GET project, financed by the ANR, will pursue the development of the electronic system; the scope of the project includes several instruments, that will utilize the final product. This ANR project injects a strong impulse into the whole active target programme, providing a very solid base for ACTAR. The ANR has financed the GET project for 515,224 € (of the 545,814 € requested), covering the expenses for material and missions, and 44 man-months of manpower in CDDs.

GET also represents a commitment from the participating partners. Concerning the French laboratories, and besides the 44 man-months mentioned above (18 at IRFU, 26 at GANIL), IRFU provides a total of 114 man-months of permanent personnel on four years; CENBG contributes for 80 man-months, and GANIL for 88 (of the latter, 18 are on CDD).

Thanks to the support of the GET ANR and the recent inclusion into the SPIRAL2

Table 5: Summary of estimated manpower, in man-months (2009 and 2013 are on six months).

	2009	2010	2011	2012	2013	Total
Phy	12.6	25.8	28.2	21.6	10.8	99.0
Eng	3.0	6.6	2.4	10.8	4.8	27.6
Tec	1.5	4.8	9.0	7.8	1.5	24.6
Total	17.1	37.2	39.6	40.2	17.1	151.2

Table 6: Manpower for the ACTAR project, by semester, and total man-months (MM).

WP	Number	Function	2/2009	1/2010	2/2010	1/2011	2/2011	1/2012	2/2012	1/2013	MM
WP1	4×Phy	Project coordination	10%	10%	10%	10%	10%	10%	10%	10%	19.2
WP2	1×Phy	WP coordination	10%	10%	10%	10%	10%	10%	10%	10%	4.8
WP2.1	4×Phy	Physics cases	10%	10%	10%	10%	10%	10%	10%	10%	19.2
WP2.2	1×Phy	Simulations	50%	50%	50%	50%	50%	50%	50%	50%	24.0
WP3	1×Phy	Physics coordination	10%	10%	10%	10%	10%	10%	10%	10%	4.8
	1×Phy	Tests	50%	50%	50%	50%	50%				15.0
	1×Eng	Technical coordination	50%	50%	50%	5%	5%				9.6
WP3.1	1×Tec	Support tests	10%	10%	10%						1.8
WP3.2	1×Tec	Design, support tests	10%	10%	10%	10%					3.0
WP3.3	1×Eng	Support experiment					10%	10%	10%	10%	1.2
	1×Tec	Support experiment					10%	10%	10%	10%	1.2
WP4	1×Phy	Physics coordination			10%	10%	10%	10%	10%	10%	3.6
	1×Eng	Technical coordination			10%	20%	10%	10%	10%	10%	4.2
WP4.1	1×Tec	Design, construction			30%	30%	30%	30%			7.2
WP4.2	1×Tec	Design, construction			30%	30%	30%	30%			5.4
WP4.3	1×Phy	Design, purchase			20%	20%	10%	10%	10%	10%	3.6
WP4.4	1×Eng	Coordination, purchase					20%	20%	20%	20%	3.6
WP4.5	1×Eng	Assembly, commissioning					50%	50%	50%	50%	9.0
	1×Tec	Support					20%	20%	20%	20%	3.6
WP5	1×Phy	Task coordination	10%	10%	10%	10%	10%	10%	10%	10%	4.8
	1×Tec	Support	5%	5%	5%	5%	5%	5%	5%	5%	2.4
										Total	151.2

Preparatory Phase, the ACTAR collaboration can enter into a phase of negotiations in view of a signature of the MoU, and at the same time start the procedure for acquiring the funds for the project.

In this respect, the evaluation of the project by the Scientific Council of the IN2P3, when positive, represents an important step to generate a real commitment of the different partner laboratories and institutes to start this negotiation phase. We would like to have such an evaluation, and possible suggestions on both the scientific and the organizational aspects.

When this first phase is completed, within a year, we will be able to present a detailed work plan with the participation of each partner to the required resources.

A Energy loss of ions

In this appendix we have collected data concerning the energy loss of ions in gases of interest for ACTAR. The figures have been obtained from table calculated using SRIM [55]. A comparison with the results of simulations made using ActarSim, which is based on the CERN package GEANT4 [70], has shown that the differences for the light particles are negligible, while discrepancies up to a factor of two have been seen for medium-mass ions (Ni). The ions for which data are shown are representative of the physics cases presented in section 4. The gases are C_4H_{10} , D_2 and a mixture of 95% He and 5% CF_4 . In all cases, a pressure of 1 bar was assumed; for other pressures, the plotted quantities (range and energy loss) scale linearly.

Fig. 22 shows the range of ions as function of their energy. This relation can be used in ACTAR to obtain the energy of particles stopped in the gas from their range. The *straggling* is not indicated in the figure; its value is calculated by SRIM to be less than 5% of the range, thus inducing a corresponding uncertainty on the measurement of the energy. The functions have a similar behaviour for the three gases, as expected, with a scaling factor due to the different densities, or more properly to the different number of electrons which can absorb the energy of the traversing particles. The same holds for the quantities presented in the following figures.

In Fig. 23 the specific energy loss dE/dx of the particle is plotted as function of its energy. These graphs are useful to compare the energies deposited by the various particles in different areas of the detector, for example close to the reaction vertex, where their energies can be estimated.

Finally Figs. 24 and 25 give dE/dx as function of the range of the particle. From these plot one can deduce the effective energy deposited by unit length on the detector, and thus the amplitude of the signals which are expected on the pads.

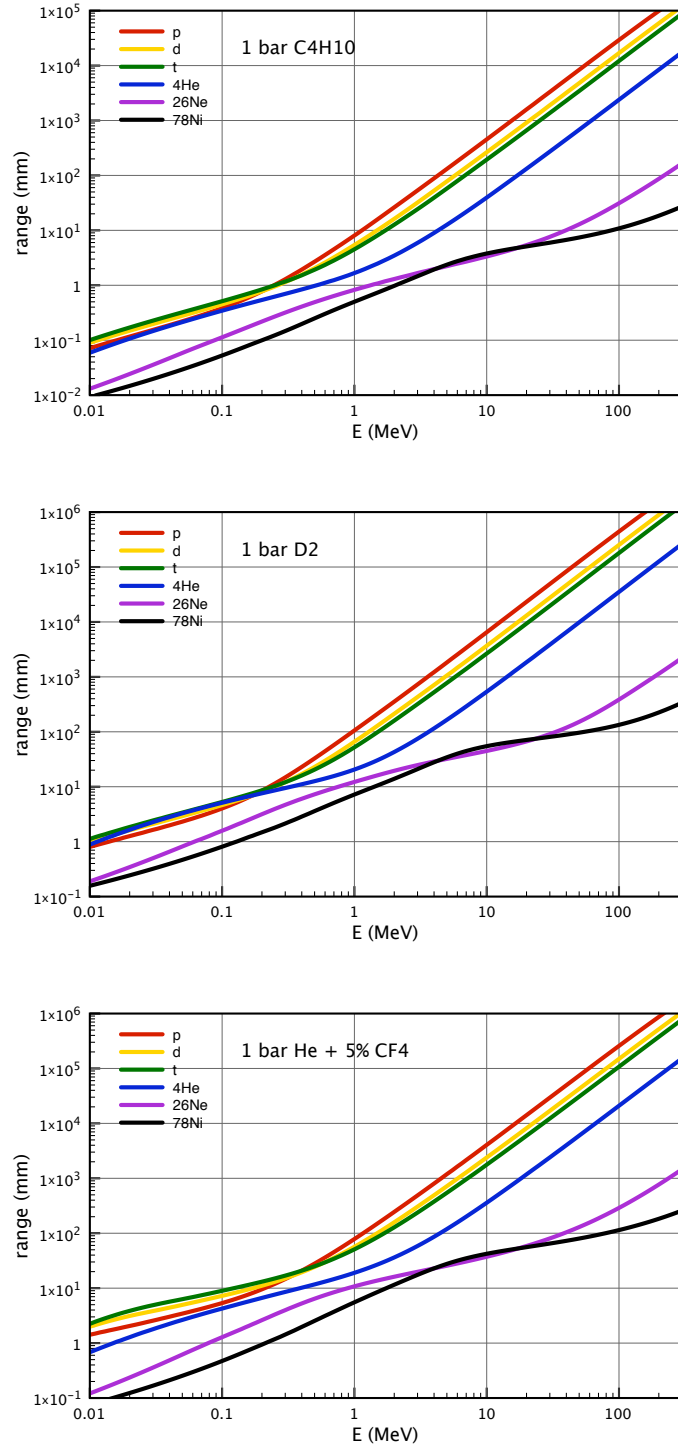


Figure 22: Range of particles in gases of interest for ACTAR.

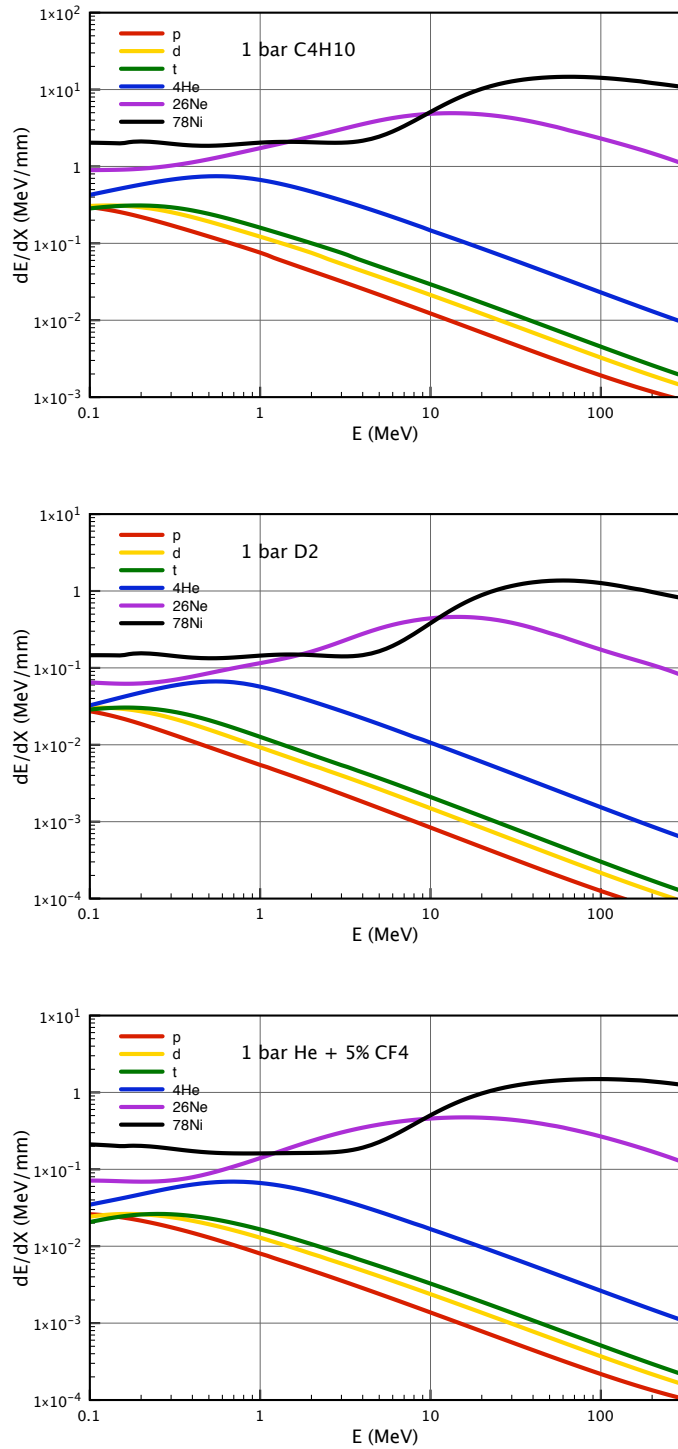


Figure 23: Energy loss of particles in gases as function of their energy.

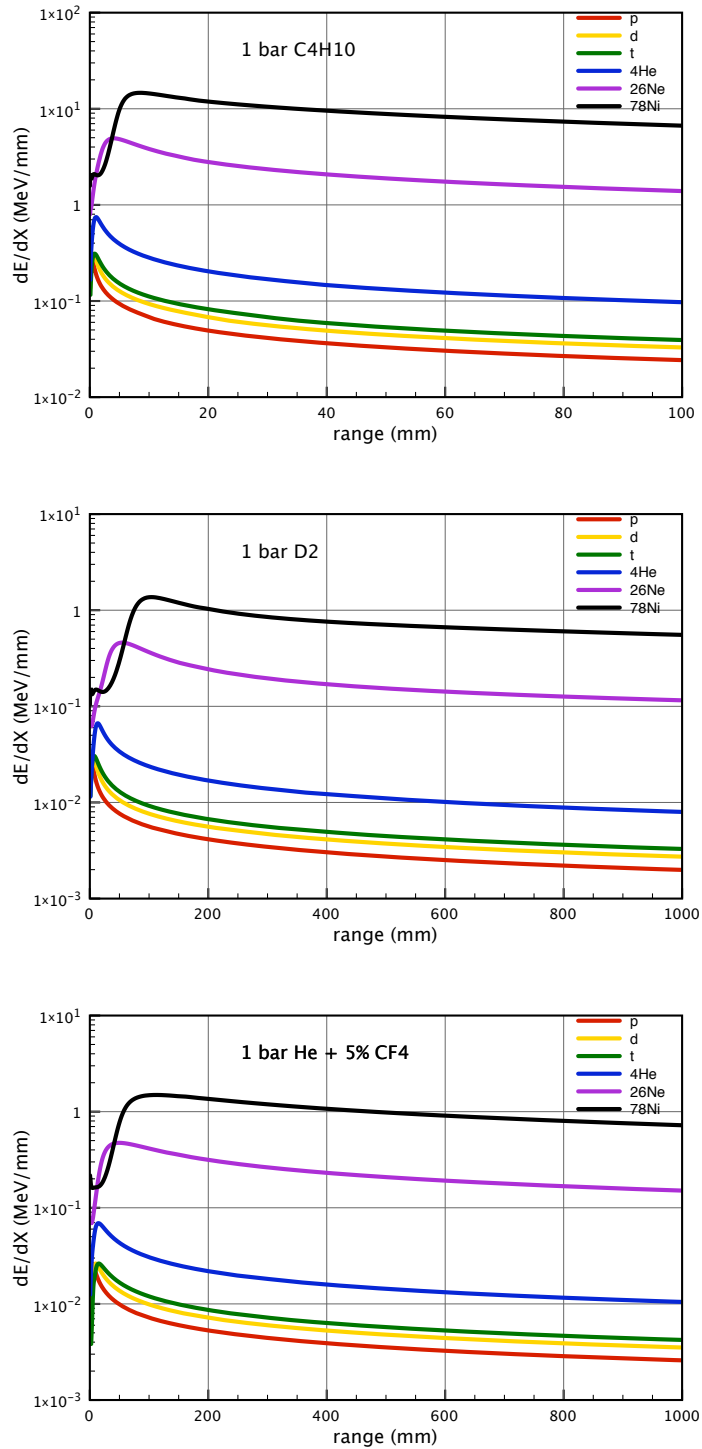


Figure 24: Energy loss of particles in gases as function of their range.

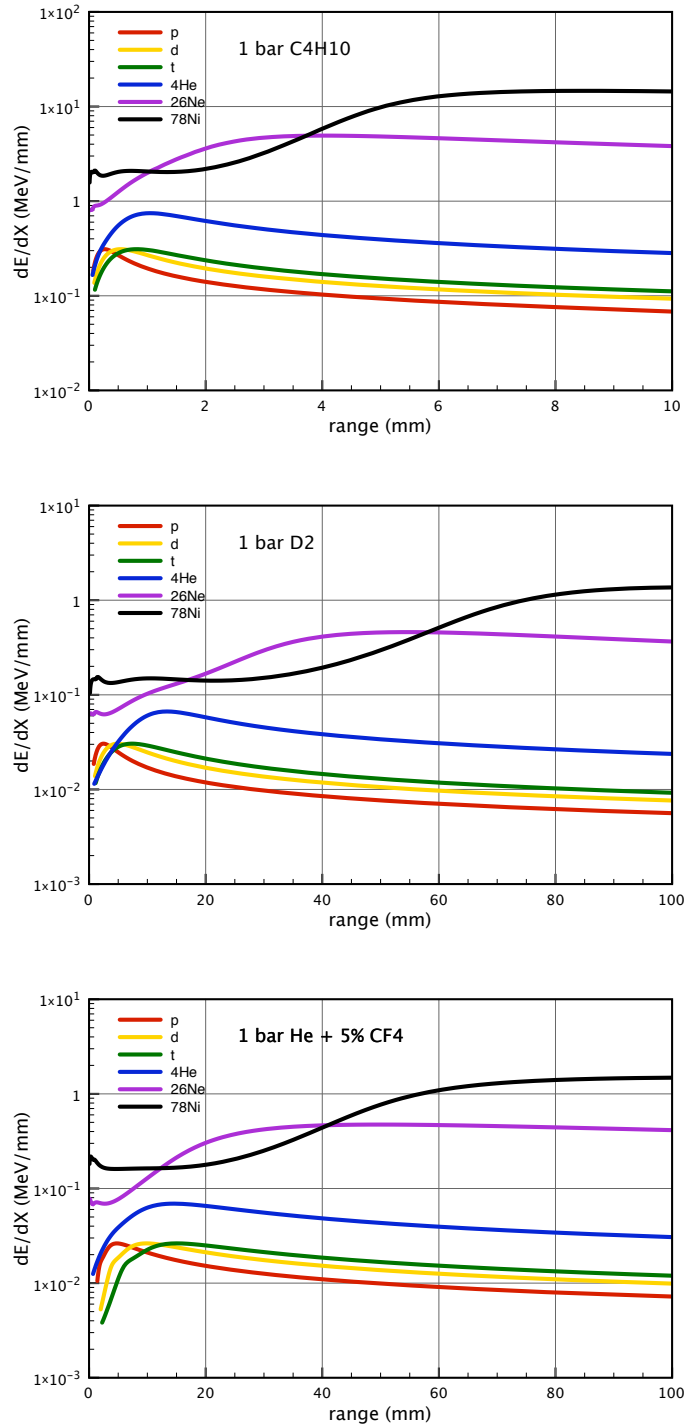


Figure 25: Energy loss of particles in gases as function of their range (detail).

References

- [1] I. Tanihata *et al.*, Phys. Rev. Lett. **55**, 2676 (1985).
- [2] W. Greiner, J. Y. Park, and W. Scheid, *Nuclear Molecules* (World Scientific, Singapore, 1995).
- [3] O. Sorlin and M. G. Porquet, Prog. Part. Nucl. Phys. **61**, 602 (2008).
- [4] B. Blank and M. Ploszajczak, Rep. Prog. Phys. **71**, 046361 (2008).
- [5] The ACTAR JRA: ns.ph.liv.ac.uk/ns-instrum-actar.html.
- [6] The GET project: groups.nscl.msu.edu/tpc/wiki/doku.php?id=electronics.
- [7] The AT-TPC at MSU: groups.nscl.msu.edu/tpc/wiki/doku.php.
- [8] The SAMURAI proposal: rarfaxp.riken.go.jp/RIBF-TAC05/10_SAMURAI.pdf.
- [9] The R3B active target proposal:
www.gsi.de/forschung/kp/kr/R3B/Technical%20Proposal.pdf.
- [10] Letters of Intent for SPIRAL2:
www.ganil.fr/research/developments/spiral2/loi_spiral2.html.
- [11] SPIRAL2 Preparatory Phase: spiral2pp.slcj.uw.edu.pl.
- [12] J. A. MacDonald (ed.), *The Time Projection Chamber* (AIP Conf Proc. Vol. 108, New York, 1984).
- [13] W. R. Leo, *Techniques for Nuclear and Particle Physics Experiments* (Springer-Verlag, New York, 1994).
- [14] G. D. Alkhazov *et al.*, Phys. Rev. Lett. **78**, 2313 (1997).
- [15] A. V. Dobrovolsky *et al.*, Nucl. Phys. A **766**, 1 (2006).
- [16] S. R. Neumaier *et al.*, Nucl. Phys. A **712**, 247 (2002).
- [17] C. E. Demonchy *et al.*, Nucl. Instrum. Methods Phys. Res. A **573**, 145 (2007).
- [18] J.-C. Santiard *et al.*, Gasplex: a low-noise analog signal processor for readout of gaseous detectors, <http://cdsweb.cern.ch/record/272783/files/ecp-94-017.pdf>, CERN-ECP-94-17, 1994.
- [19] M. Caamaño *et al.*, Phys. Rev. Lett. **99**, 062502 (2007).
- [20] M. Caamaño *et al.*, Phys. Rev. C **78**, 044001 (2008).
- [21] I. Tanihata *et al.*, Phys. Rev. Lett. **100**, 192502 (2008).
- [22] T. Roger *et al.*, Phys. Rev. C **79**, 031603(R) (2009).
- [23] C. Monrozeau *et al.*, Phys. Rev. Lett. **100**, 042501 (2008).
- [24] B. Blank *et al.*, Nucl. Instrum. Methods Phys. Res. B **266**, 4606 (2008).
- [25] F. Sauli, Nucl. Instrum. Methods Phys. Res. A **386**, 531 (1997).
- [26] J. Giovinazzo *et al.*, Phys. Rev. Lett. **99**, 102501 (2007).
- [27] A. M. Laird *et al.*, Nucl. Instrum. Methods Phys. Res. A **57**, 306 (2007).
- [28] The TACTIC detector: tactic.triumf.ca.
- [29] The ANASEN detector: www.nscl.msu.edu/prop/exp/anasen.
- [30] M. D. Heffner, P. D. Barnes, and J. L. Klay, Innovative Fission Measurements with a Time Projection Chamber, Lawrence Livermore National Laboratory, UCRL-TR-217600, e-reports-ext.llnl.gov/pdf/327870.pdf, 2005.

- [31] Y. Giomataris, P. Rebourgeard, J. Robert, and G. Charpak, Nucl. Instrum. Methods Phys. Res. A **376**, 29 (1996).
- [32] F. Sánchez and the NEXT Collaboration, Nucl. Phys. B-Proc. Sup. **188**, 71 (2009).
- [33] G. D. Alkhazov *et al.*, Nucl. Phys. A **712**, 269 (2002).
- [34] P. Egelhof *et al.*, Eur. Phys. J. A **15**, 27 (2002).
- [35] A. M. Bernstein, V. R. Brown, and V. A. Madsen, Comments Nucl. Part. Phys. **11**, 203 (1983).
- [36] E. Khan *et al.*, Phys. Lett. B **490**, 45 (2000).
- [37] L. Gaudefroy *et al.*, Phys. Rev. Lett. **97**, 092501 (2006).
- [38] W. N. Catford *et al.*, Eur. Phys. J. A **25** s01, 245 (2005).
- [39] E. Pollacco *et al.*, Eur. Phys. J. A **25** s01, 245 (2005).
- [40] G. V. Rogachev *et al.*, Phys. Rev. C **67**, 041603 (2003).
- [41] M. Freer, Rep. Prog. Phys. **70**, 2149 (2007).
- [42] L. Axelsson *et al.*, Phys. Rev. C **54**, R1511 (1996).
- [43] M. Freer *et al.*, Phys. Rev. Lett. **96**, 042501 (4 pages) (2006).
- [44] H. Ishiyama *et al.*, Phys. Lett. B **640**, 82 (2006).
- [45] M. N. Harakeh and A. van der Woude, *Giant Resonances: Fundamental high frequency modes of nuclear excitation* (Oxford University Press, Oxford, 2001).
- [46] T. Li *et al.*, Phys. Rev. Lett. **99**, 162503 (2007).
- [47] A. Leistenschneider *et al.*, Phys. Rev. Lett. **86**, 5442 (2001).
- [48] P. Adrich *et al.*, Phys. Rev. Lett. **95**, 132501 (2005).
- [49] J. Gibelin *et al.*, Nucl. Phys. A **788**, 153c (2007).
- [50] J. Görres, M. Wiescher, and F.-K. Thielemann, Phys. Rev. C **51**, 392 (1995).
- [51] H. Alvarez Pol, ActarSim: a simulation program for ACTAR: fpsalmon.usc.es/r3b/ActarSimACTAR.shtml.
- [52] A. Obertelli *et al.*, Phys. Lett. B **633**, 33 (2006).
- [53] J. R. Terry *et al.*, Phys. Lett. B **640**, 86 (2006).
- [54] J. C. Dalouzy *et al.*, Phys. Rev. Lett. **102**, 162503 (2009).
- [55] J. F. Ziegler, J. P. Biersack, and U. Littmark, *The Stopping and Range of Ions in Solids* (Pergamon Press, New York, 1985).
- [56] M. Hunyadi *et al.*, Phys. Lett. B **576**, 253 (2003).
- [57] B. F. Davis *et al.*, Phys. Rev. Lett. **79**, 609 (1997).
- [58] B. K. Nayak *et al.*, Phys. Lett. B **637**, 43 (2006).
- [59] M. Hunyadi *et al.*, Phys. Rev. C **75**, 014606 (2007).
- [60] K. Miernik *et al.*, Phys. Rev. Lett. **99**, 192501 (2007).
- [61] R. Veenhof, Garfield – simulation of gaseous detectors, CERN program library W5050.
- [62] S. F. Biagi, Nucl. Instrum. Methods Phys. Res. A **421**, 234 (1999).
- [63] A. Bay *et al.*, Nucl. Instrum. Methods Phys. Res. A **488**, 162 (2002).
- [64] A. Delbart *et al.*, Nucl. Instrum. Methods Phys. Res. A **461**, 84 (2001).
- [65] I. Giomataris *et al.*, Nucl. Instrum. Methods Phys. Res. A **560**, 405 (2006).

- [66] G. Charpak, J. Derré, Y. Giomataris, and P. Rebourgeard, Nucl. Instrum. Methods Phys. Res. A **478**, 26 (2002).
- [67] Y. Ivaniouchenkov, P. Fonte, V. Peskov, and B. D. Ramsey, Nucl. Instrum. Methods Phys. Res. A **422**, 300 (1999).
- [68] M. S. Dixit and A. Rankin, Nucl. Instrum. Methods Phys. Res. A **566**, 281 (2006).
- [69] Y. Giomataris, Nucl. Instrum. Methods Phys. Res. A **419**, 239 (1998).
- [70] S. Agostinelli *et al.*, Nucl. Instrum. Methods Phys. Res. A **506**, 250 (2003).